applied sciences

MDPI

Article

Effects of Central Cut Width on the Dynamical Characteristics of Box Assembly Structure

Christopher Padilla, Antonio Flores †, Ezekiel Granillo †, Jonah Madrid † and Abdessattar Abdelkefi *

Department of Mechanical and Aerospace Engineering, New Mexico State University, Las Cruces, NM 88003, USA; crispy3@nmsu.edu (C.P.); tonyflo@nmsu.edu (A.F.); jonahmad@nmsu.edu (J.M.)

* Correspondence: abdu@nmsu.edu

† These authors contributed equally to this work.

Abstract: An investigation into the Box Assembly with Removable Component (BARC) structure is conducted by utilizing computational simulations and experimental structural testing in order to determine the complex dynamical responses instigated by the central cut of the system. Because the dynamics of the BARC system is complex, this study focuses primarily on analyzing the behavior of the box assembly (BA) system. The investigation explores the dynamics of the BA system by varying the central cut widths, ranging from a cut as wide as 0.5″ cut to a 0.25″ cut system, as well as a 0.1″ cut and a system with no cut at all. Experimental testing is performed on each system including a free vibration test using an impact hammer to excite and identify the dominant frequencies of each structure. This testing is followed by pseudo-random vibration tests and swept sinusoidal excitation tests to determine the nonlinear aspects of these systems, such as the possible existence of nonlinear softening, hardening, and/or damping. The results show that nonlinear softening and nonlinear damping are present in each system. The no-cut system demonstrated the highest peak frequencies throughout all the tests, being the most rigid structure. The 0.25″ cut system was shown to have the highest peak frequencies among all the cut systems in both the finite elemenet analysis (FEA) and impact testing. This trend did not continue, though, in the random and harmonic testing, possibly due to the added stiffness of the test setup with the slip table and stinger. The results show the importance of accurately measuring the central cut width and how possible geometric uncertainties change the overall dynamical behaviors of complex systems, such as natural characteristics, nonlinear responses, coupling of modes, and oscillating amplitudes.

Keywords: BARC; cut width; FEA; experimental structural dynamics; nonlinear dynamics

check for updates

Academic Editor: Jean-Jacques Sinou

Received: 21 November 2024
Revised: 20 December 2024
Accepted: 25 December 2024
Published: 4 January 2025

Citation: Padilla, C.; Flores, A.; Granillo, E.; Madrid, J.; Abdelkefi, A. Effects of Central Cut Width on the Dynamical Characteristics of Box Assembly Structure. *Appl. Sci.* **2025**, *15*, 417. https://doi.org/10.3390/app15010417

Copyright: © 2025 by the authors. Licensee MDPI, Basel, Switzerland. This article is an open access article distributed under the terms and conditions of the Creative Commons Attribution (CC BY) license (https://creativecommons.org/licenses/by/4.0/).

1. Introduction

Modal testing enables the understanding of the dynamics within complex systems by subjecting these systems to a laboratory environment, closely replicating a service environment [1–3]. In doing so, modal testing grants a cost-effective alternative to field-testing, allowing for a minimization of uncertainties and greater control of the test subject. During laboratory testing, efforts are made to replicate a system's service environment as much as possible for the best results. It can prove challenging to mimic vibration testing environments as they may occur only during large scale events, such as earthquakes and mining activities [4,5]. While doing so, one factor within the test changes at a time, giving an insight into how the dynamics of the system react to these changes. Transitioning from the laboratory to the field does pose challenges and verify knowledge of the system, as discussed by Varoto in [6].

Typically, dynamical testing is a very complex process. There are multiple points of interest within one system, giving researchers a difficult time trying to understand each point within a singular assembly. Running experiments on entire assemblies is often very difficult and expensive. Because of this, it is common to see researchers implement a substructuring approach that assists in the testing of various systems. Dynamic substructuring allows for the break-up of the system into individual components and characterizes the dynamical behaviors of these components by themselves, thus eventually understanding the behaviors of each component [7,8]. Once the behaviors of each component are understood, researchers can rebuild the assembly back into the complete system with a better understanding of the complete dynamics due to substructuring. A common method of substructuring is a frequency-based substructuring approach with the goal of predicting the dynamical behavior of a system using its components through frequency response functions [9–11]. Another method commonly used in structural dynamics is component mode synthesis. This method has played a significant role in identifying dynamical behaviors of systems that are too difficult to analyze in their entirety [12]. When utilizing this substructuring method, local dynamical behavior is identified more easily than when testing the entire system since the smaller component is monitored more closely at an individual scale. A final substructuring approach to be considered for this study is the Craig–Bampton method. This method is based on creating reduced-order models of subparts for the assembly [13,14]. This is relevant for creating reduced-order systems, but does not incorporate contact interferences, which will be seen and discussed in the experimentation section of this study. Other types of analysis include hybrid system analysis [15,16], but the primary focus of the work carried out was on dynamic substructuring and frequency-based substructuring.

This current work is conducted by investigating the linear and nonlinear characteristics within each system under consideration. A system can be determined to be linear or nonlinear by investigating the relationship between the input and output of the system. If a system has an output that corresponds to a specific input of the system, then that system is considered linear. If this relationship does not exist and there is no correspondence, the system becomes more complicated and is considered nonlinear [17,18]. Various forms of nonlinearities can occur in a system including nonlinear damping, nonlinear hardening, and/or nonlinear softening. Nonlinear damping is considered a primary source of nonlinearity in numerous systems, which can be caused by many properties intrinsic to a system. Some of these can include geometry, material properties, and bolted-joint connections. Typically, as excitation increases in a system, the nonlinear damping force may also increase or decrease [19]. Nonlinear softening and hardening occur when the responses of the system bend one way or the other when the input excitation is increased. Typically, when frequency response curves show an increase in frequency, nonlinear hardening is present. When frequency response curves show a bend to the decrease in frequency, nonlinear softening is present [20,21].

To further understand the relationship between nonlinearities and substructured components, a system with enough complexity and connections had to be developed. The Box Assembly with Removable Component (BARC) system was a collaboration of effort between researchers at both Sandia National Laboratories and the Kansas City National Security Campus which has led to an extensive study into its dynamical behaviors during shock, vibration, and modal tests [22]. It was initially introduced as a test article to evaluate fixture influence within different dynamic environments. The BARC is designed to mimic real-world testing conditions, where the system is made of a flexible box assembly and a removable component that represents a test article [23]. This is similar to that of aircraft engines mounted to a flexible wing or other payloads where the influence of the wing on the engine's dynamics would like to be understood. To replicate real-world scenarios,

researchers carefully define boundary conditions and establish experimental setups to study the structure. Prior research on the system has demonstrated the importance that bolted connections and boundary conditions have on the dynamic response of the system, including nonlinear behaviors observed during modal testing and finite element analysis (FEA) [24]. Extensive research on various boundary conditions, including different hole configurations for bolted-joint connections, has provided insights into the system's behavior under various environmental tests, such as varying boundary conditions of the BARC itself [25,26].

Prior to the introduction of the BARC, components were subjected to dynamical testing on rigid structures. This method typically fails to replicate real-world service environments, where components are subject to various degrees of flexibility. Some common examples include a missile attached to a jet wing or a CubeSat docking on a larger satellite [27]. The BARC allows for a structure that can simply replicate a service environment for specific components. Efforts have been and are currently being made to have a valuable understanding of the complexities of the BARC system, where researchers are continuously striving to enhance their grasp of its behavior under various testing conditions. Some of this research includes varying the size of the BARC and conducting multi-axis testing on the system [28,29].

Research studies on the BARC have been conducted previously, but, to the authors' knowledge, no deep investigation on the changing of the size of the central cut has been conducted. Studies have shown two distinct iterations of the cut size, being an investigation with a no-cut case [22,30] and studies with a common 0.5" cut case [31,32]. Prior work studying a BARC with a different cut width has not been shown. In this work, a configuration with a 0.25" cut is selected due to it being the intermediate point between the no-cut and traditional 0.5" cut system. The smallest cut that could be made on the Box Assembly (BA) is the 0.1" thin cut. This is performed to compare the influence of just a thin cut as opposed to bigger cuts. It is not uncommon to see the removal or addition of mass to a system to influence its dynamical characteristics. The same purpose is investigated with the introduction of these two new cut systems. A recent conference paper by the authors has shown some preliminary results on the influence of the cut width on the dominant frequencies of the full BARC system [33]. This current study aims to comprehensively explore the effects of the cut width on the dynamical characteristics of the box assembly system. In particular, this effort would like to examine how uncertainty in the central cut of the BA may influence the dynamical properties (frequencies, mode shapes, coupling between modes, nonlinear behaviors, and oscillating amplitudes) of the system. Current models, such as proper orthogonal decomposition (POD), exist to extract mode shapes for a vibratory system using reduced-order modeling. This exact method provided insight during the investigation, but was not directly applied [34].

Establishing standardized experimental testing conditions for the BARC is important for the accurate comparisons of results across studies to ensure the reliability and validity of findings. Additionally, researchers are adamant about exploring the effects of the central cut within the BARC system, recognizing that it has the potential to introduce discrepancies that have not yet been fully understood. Such examples of discrepancies may include differences in peak frequencies and trends in the nonlinear behavior of the systems. Through an investigation into the effects of various cut sizes, this research aims to identify the linear and nonlinear characteristics of box assembly systems with various cut widths that will enable accurate comparisons among studies and allow for easier reproduction of results. To assess the system's response, various excitation directions are evaluated, providing insights into how the system behaves under different circumstances [32,35]. Random and harmonic vibration tests are conducted on each system, as well as a free

vibration impact test. Moreover, FEA is carried out to determine the vibrational modes and natural frequencies and qualitatively understand the dynamics of each system and the possible presence of mode switching [36]. The rest of this study is composed of several sections including the configurations considered, experimental techniques, computational analysis, and results with a particular focus on the effects of the central cut width on the dynamical characteristics of the box assembly system.

2. Box Assembly Configurations and Experimental Techniques

To investigate the effects of the width of the central cut of the BA structure on the dynamical responses of the system, four configurations of the central cut were considered, as presented in Figure 1. These configurations included the original BA structure with a 0.5″ cut shown in Figure 1a, and three modified designs (Figure 1b–d), namely, BA with a 0.25″, 0.1″, and 0″ central cut. The 0″ central cut was named as no-cut configuration, as shown in Figure 1d. The three width cut cases of 0.5″, 0.25″, and 0.1″ can be seen as input uncertainties in the design and manufacturing of the box assembly system.

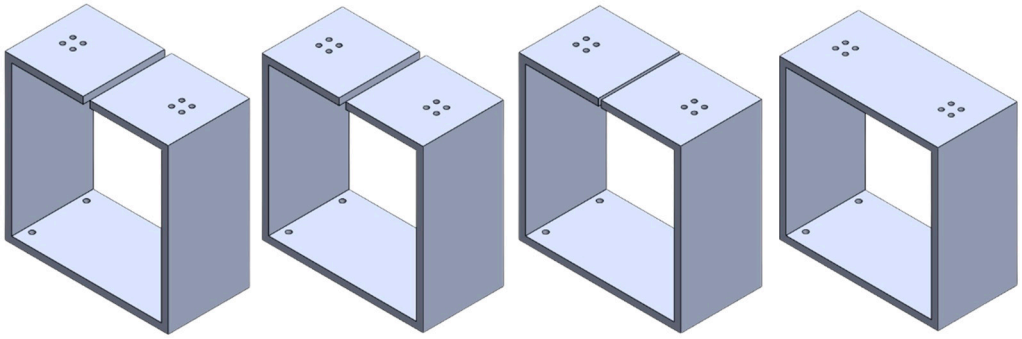

Figure 1. Box assembly configurations under consideration: (**a**) 0.5″ cut, (**b**) 0.25″ cut, (**c**) 0.1″ cut, and (**d**) 0″ cut.

To gain a further understanding of the influence of the central cut on the dynamics of the box assembly systems under investigation, finite element analysis (FEA) was carried out through the 3DExperience's ABAQUS software (3DEXPERIENCE R2023x, Dassault Systèmes). The computational outcomes from FEA are valuable and can be used as a reference for the identification of the linear properties (natural frequencies and mode shapes) of the systems under consideration. This is beneficial in terms of guiding the experiments, particularly harmonic testing, to be performed near resonances where most of the important characteristics can be identified.

Because two accelerometers were attached to the box assembly in the experimental measurements, it was important to computationally model the accelerometers in their specific locations so a better quantitative comparison could be performed between the FEA and experimental results. For this reason, finite element simulations were conducted on both assembly systems with and without accelerometers. For the FEA with the presence of accelerometers, two accelerometers weighing 6.3 g each were placed on every system in the respective locations as in the experiments, as shown in Figures 2 and 3. These accelerometers are defined as the "top" and "side" accelerometers for the remainder of this study. Previous research in the literature, as well as FEA, have shown these locations for the accelerometers to be the ideal locations to capture high dynamic responses of the system [24]. A structural simulation was selected to focus on purely the structural dynamics of the system. Next, a mesh was manually initialized in the software. A tetrahedron mesh was selected with the initial elements of 10mm and of quadratic order. The order allows for an additional node between the standard vertices used in a tetrahedron model. A sag

ratio of 0.1 was selected to minimize the distance between the elements and the edge of the model. Then, this finite element model (FEM) was subjected to a frequency step analysis. Restrictions were imposed on the translation in X-, Y-, and Z-directions within the holes of the BA's base plate. A mesh convergence analysis was carried out by iteratively reducing element size and maintaining a sag ratio of about an order of magnitude. It was determined that 400,000 elements are enough to accurately estimate the natural frequencies and mode shapes of the box assembly systems.

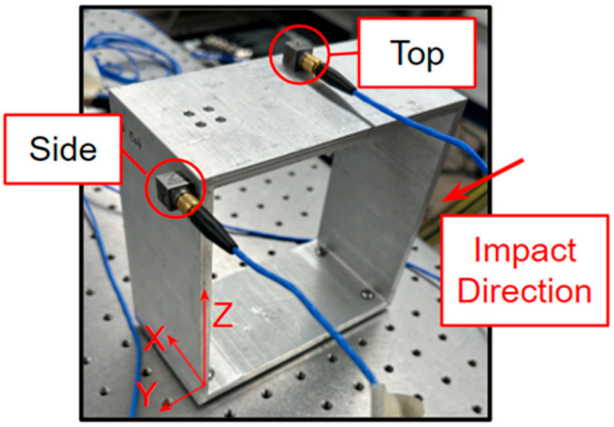

Figure 2. Box assembly free vibration test setup.

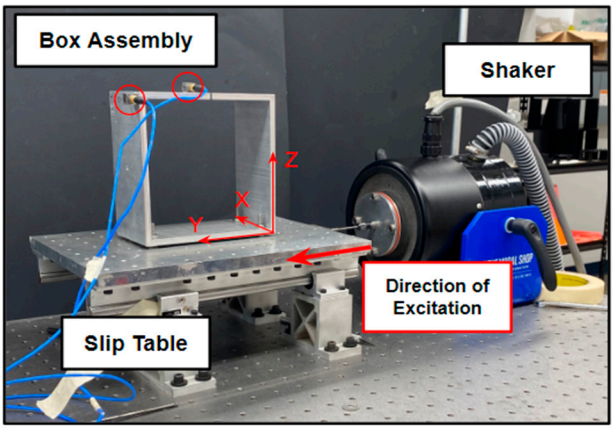

Figure 3. Box assembly random and harmonic test setup.

The dominant frequencies of the box assembly systems under consideration were estimated through a free vibration test by hitting the system with a modal impact hammer with a blue soft tip. In order to excite the first mode of each system, the BA was impacted in the Y-direction, as indicated in Figure 2. It should be mentioned that spacers were used at the bolted connections on the base of each system to accurately explore the dynamics of the systems with the considered set of boundary conditions [24]. In fact, the inclusion of the space nuts prevented any interference between the box assembly base motion and the table holding it. In this way, the box assembly could freely vibrate beyond the horizontal plane.

To achieve a comprehensive insight into the dynamics of the four box assembly configurations and how the central cut influences the dynamical properties of these systems, pseudorandom vibration tests were performed in the Y-direction with four increasing levels of excitation. The experimental setup for random excitation is depicted in Figure 3. This setup consists of an extended slip table with a stinger attached to a smart table. The BA structures were fixed to the extended slip table via a bolted-joint connection. In addition to the two main accelerometers attached to the box assembly, an additional accelerometer served as a reference point on the base of the slip table.

This random experimental testing is beneficial in order to understand the effects of the central cut on the dynamical properties of the box assembly system. This experimental testing leads to (1) detecting the dominant frequencies in these box assembly systems; (2) determining if there is any nonlinear softening or hardening in the different modes of vibration; and (3) examining the possible presence of nonlinear damping. Indeed, by increasing the level of the input excitation, the resonant frequencies may change and hence, the existence of nonlinear softening/hardening can be detected in a qualitative manner. Additionally, the existence of nonlinear damping can be seen by plotting the output-to-input frequency response curves for the different levels of excitations.

In order to quantitatively determine the influence of the central cut on the dynamics of the box assembly system, a stepped-sine harmonic vibration testing was then performed, focusing on the excitation frequencies near the fundamental resonance and when considering various levels of the input excitation amplitudes. In this way, quantitative detection of the presence of nonlinear damping, softening, and/or hardening could be accurately identified. A particular focus was paid to the top and side accelerometers in terms of behaviors. In this study, four levels of increasing excitation amplitudes were examined to possibly activate the nonlinear regime of the systems under consideration. The setup for harmonic testing is nearly identical to random vibration testing, as presented in Figure 3.

3. Effect of the Central Cut on the Box Assembly Characteristics: Computational Modeling

To determine a range of natural frequencies for the box assembly systems when different central cut values are considered, finite element simulations were carried out on each system using 3DExperience ABAQUS finite element analysis. Typically, finite element models do not consider the influence of the accelerometer on the system [22,30]. In [24], the authors have demonstrated that the inclusion of accelerometers induces a mass loading on the system. Because of this, simulations were run both with and without accelerometers. Tables 1–5 depict and tabulate the mode shapes for the first four modes for the cases without (Tables 1 and 2) and with accelerometers (Tables 3–5). For the cases without accelerometers, Table 1 shows the first four mode shapes of each of the four systems being examined. It is noted that each of the box assembly systems with a central cut exhibits identical mode shapes without the presence of mode switching. Additionally, similarities are seen between the modes of the systems with a cut versus the system with no cut.

Table 1. Mode shapes without accelerometers found through FEA.

	**Mode 1**	**Mode 2**	**Mode 3**	**Mode 4**
0.5″ Cut	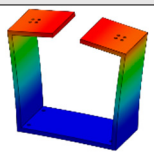 (Dominant bending)	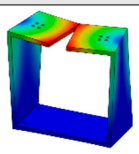 (Dominant torsional)	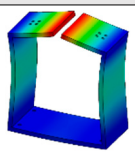 (Dominant bending)	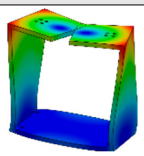 (Dominant torsional)
0.25″ Cut	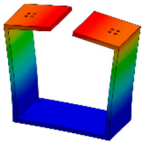 (Dominant bending)	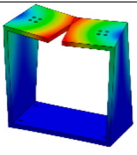 (Dominant torsional)	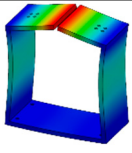 (Dominant bending)	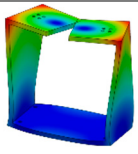 (Dominant torsional)

Table 1. *Cont.*

	Mode 1	Mode 2	Mode 3	Mode 4
0.1″ Cut	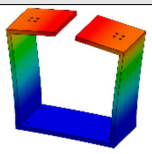 (Dominant bending)	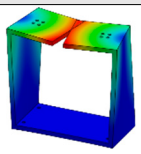 (Dominant torsional)	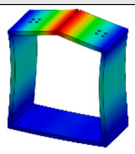 (Dominant bending)	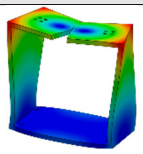 (Dominant torsional)
No Cut	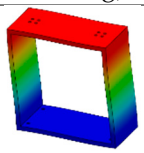 (Dominant bending)	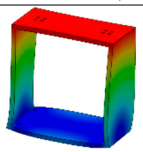 (Dominant torsional)	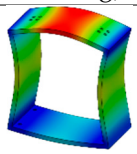 (Dominant bending)	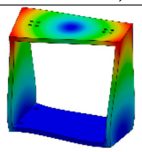 (Dominant torsional)

Table 2. Natural frequencies of the box assembly w/o accelerometers found through FEA.

	Mode 1 (Hz)	Mode 2 (Hz)	Mode 3 (Hz)	Mode 4 (Hz)
0.5″	114.117	360.968	553.397	919.342
*** 0.375″**	113.484	352.823	538.902	919.423
0.25″	112.25	344.438	524.14	913.763
*** 0.125″**	111.313	336.791	510.664	913.392
0.1″	110.820	334.730	507.221	906.566
No	186.122	676.673	759.663	928.357

* only computationally determined, no experimentation performed.

Table 3. Cases with accelerometers for modes 1 and 2 found through FEA.

	Mode 1		Mode 2	
0.5″ Cut	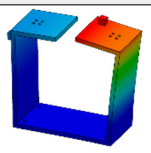 **(a)**	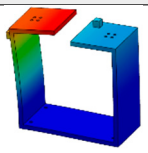 (b)	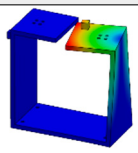 (a)	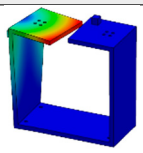 (b)
0.25″ Cut	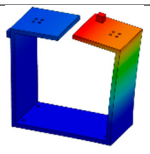 (a)	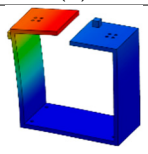 (b)	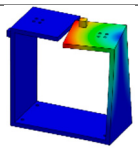 (a)	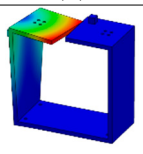 (b)
0.1″ Cut	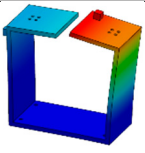 (a)	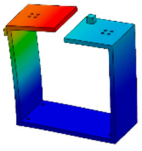 (b)	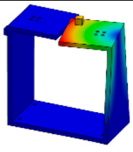 (a)	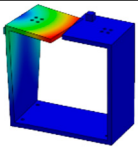 (b)
No Cut	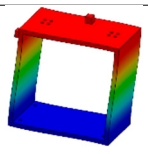		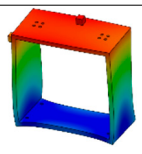	

Table 4. Cases with accelerometers for modes 3 and 4 found through FEA.

	Mode 3		Mode 4	
0.5″ Cut	**(a)**	(b)	(a)	(b)
0.25″ Cut	(a)	(b)	(a)	(b)
0.1″ Cut	(a)	(b)	(a)	(b)
No Cut				

Table 5. Natural frequencies of the box assembly with accelerometers found through FEA.

	Mode 1 (Hz)		Mode 2 (Hz)		Mode 3 (Hz)		Mode 4 (Hz)	
	(a)	**(b)**	**(a)**	**(b)**	**(a)**	**(b)**	**(a)**	**(b)**
0.5″	111.153	112.617	344.427	360.032	527.676	555.512	887.401	914.904
*** 0.375″**	110.242	111.684	336.679	352.031	513.882	540.998	887.825	915.082
0.25″	121.084	123.031	373.261	392.969	552.876	583.865	981.876	1010.030
*** 0.125″**	108.152	109.643	321.424	336.236	487.028	512.659	882.920	908.901
0.1″	107.668	109.174	319.515	334.126	483.774	509.095	876.082	902.446
No	183.117		663.664		749.612		913.189	

* only computationally determined, no experimentation performed.

Table 2 shows the tabulated natural frequencies found through the FEA of the systems without accelerometers. The no-cut system has the highest natural frequencies at 186.122 Hz, 676.673 Hz, 759.663 Hz, and 928.357 Hz respective to the mode; this is likely due to it being the most rigid out of all the systems. It is important to note that the systems with a cut show a decrease in frequency as the cut width decreases. This can be seen when comparing the cut widths at each mode. For example, at mode 2, the 0.5″ cut has a natural frequency of 360.968 Hz. When the cut width decreases to 0.25″, the natural frequency decreases to 344.438 Hz. This trend continues on to the 0.1″ cut with a natural frequency of 334.730 Hz. Another interesting note is that mode 4 of each system does not show very much decrease between cuts as the other systems, only changing around 13 Hz. Excluding mode 1, with a change of 3 Hz (since that is a low-frequency mode), modes 2 and 3 show more change in frequency as the cut width decreases, changing as much as 26 Hz in mode 2 and 46 Hz in mode 3. Mode 4 of each cut system is also comparable to the no-cut system, where this is not the case with modes 1–3. This result, when comparing the no-cut case to the cut cases, may be explained by the fact that the cut has more influence on the first three modes

than the fourth mode, as shown in Table 1. It should be mentioned that two additional configurations for the central cut width, namely, 0.375″ and 0.125″, are considered in the computational simulations in order to better understand the influence of the central cut width on the natural frequencies of the box assembly system, as indicated in Table 2.

Tables 3 and 4 indicate the mode shapes of the systems with accelerometers. The focus of this work is on these systems with accelerometers, unless otherwise specified. It can be noticed that the modes with a cut are broken up into (a) and (b). This is due to the fact that the presence of accelerometers on the system introduces asymmetry. Each mode shape is nearly identical to its (a) or (b) counterpart, the only difference being a mirror of the other about the central axis. It is important to mention that the inclusion of the accelerometers in the computational is needed in order to show the breaking of the modes due to asymmetry, and hence the possible presence of broadband regions for the modes of vibration. This behavior will be deeply studied in the harmonic analysis section.

Shown in Table 5 are the natural frequencies found through the finite element analysis for the modes shown in Tables 3 and 4. Once again, the no-cut case has the highest natural frequencies since it is the most rigid system. In this case, the 0.25″ system has the highest natural frequencies among all the systems with a cut. As a result, FEA was conducted on the systems with a cut width near the 0.25″ cut system, these being the 0.375″ cut system and the 0.125″ cut system. The goal was to determine if there is a build-up and/or build-down from the peak of the 0.25″ cut system. The results do not show this to be the case since there is a decrease from 0.5″ to the 0.375″ system, though a build-down from the 0.25″ cut system is seen as the frequencies decrease from the 0.125″ system to the 0.1″ system. This further adds to the intrigue of the system, where the 0.25″ system will be of particular interest for the remainder of this study. Similarly to the results found in Table 2, a decrease between the systems with a cut can be found, excluding the 0.25″ cut case. The decrease between the systems may be due to the additional mass loading of the accelerometers and how it influences the total mass of the box assembly structure. The results presented in Table 5 demonstrate the need to carefully measure the central cut width for box assemblies and the importance of computationally modeling the accelerometers. Indeed, a small uncertainty in the design/manufacturing of the central cut may lead to significant differences in the natural frequencies of the system and hence, the broadband regions.

4. Experimental Results Exploring Dynamics of Box Assembly Structure and Influence of the Cut Width

This section aims to investigate the effects changing the central cut width has on the system by conducting free, random, and harmonic vibration tests on each box assembly structure. Because the finite element analysis uses ideal assumptions, the simulations are utilized to gain a basic understanding of each system. The results of those tests will be introduced and discussed in this section, allowing for a deeper understanding of how the conclusions at the end of the study are reached. This will also allow other researchers to replicate the experimentation and verify the results, opening the conversation even further for how accurately measuring the central cut width of the BARC affects the dynamics of the system.

4.1. Influence of the Central Cut Width on the Dynamics of the Box Assembly Structure: Free Vibration Testing

The first set of experiments performed on each of the systems consists of a free vibration impact test, where the setup for the test is as found in Figure 2. Impact testing gives an overall look at the characteristics of each system, allowing for the dominant frequencies and mode shapes to be observed. The results are compared to the FEA to

ensure that the FEA can be used to qualitatively verify the experimental results. For this study, it should be noted that each test covers a range of frequencies that is lower than 600 Hz for all the cut systems and 800 Hz for the no-cut system. Mode 4 is shown to be nearly 900 Hz or more for each box assembly system according to the FEA (as shown in Table 5), making it difficult to repeatedly conduct tests at these high frequencies. Hence, the focus is on the first three modes for each system for the remainder of the study.

Inspecting the plots shown in Figure 4, each system with a central cut shows somewhat similar results, where the first mode of each system, modes 1(a) and 1(b), are shown as almost a "double peak" around 100 Hz. The double peak is an indication that the accelerometers are inducing an asymmetry in the box assembly system, and therefore, the presence of a resonant broadband region, which will be deeply examined in the harmonic testing section. Further, for higher modes of vibration, it is noticed that the difference between the two dominant frequencies becomes higher. This is expected, as seen through the FEA and indicated in Table 5.

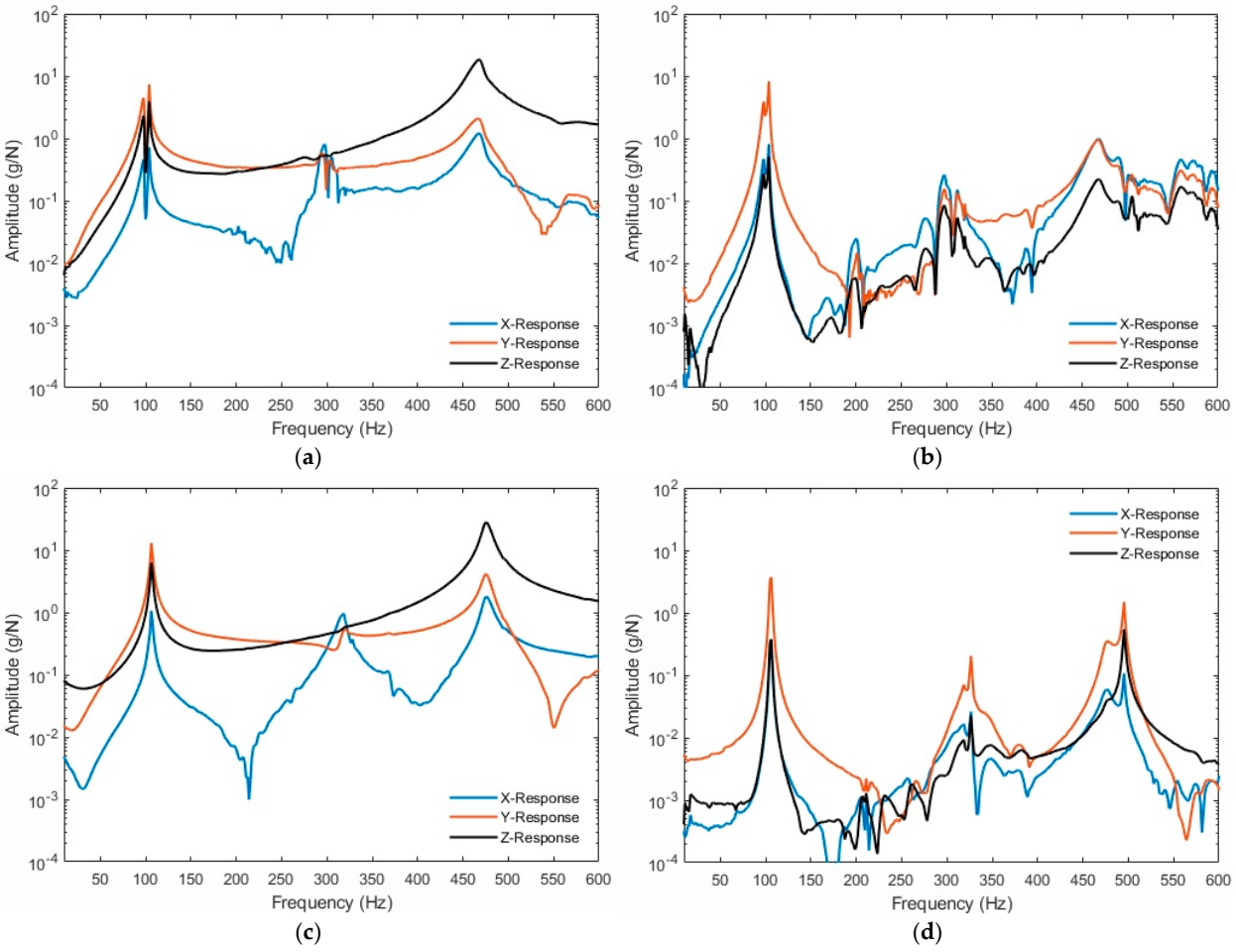

Figure 4. *Cont.*

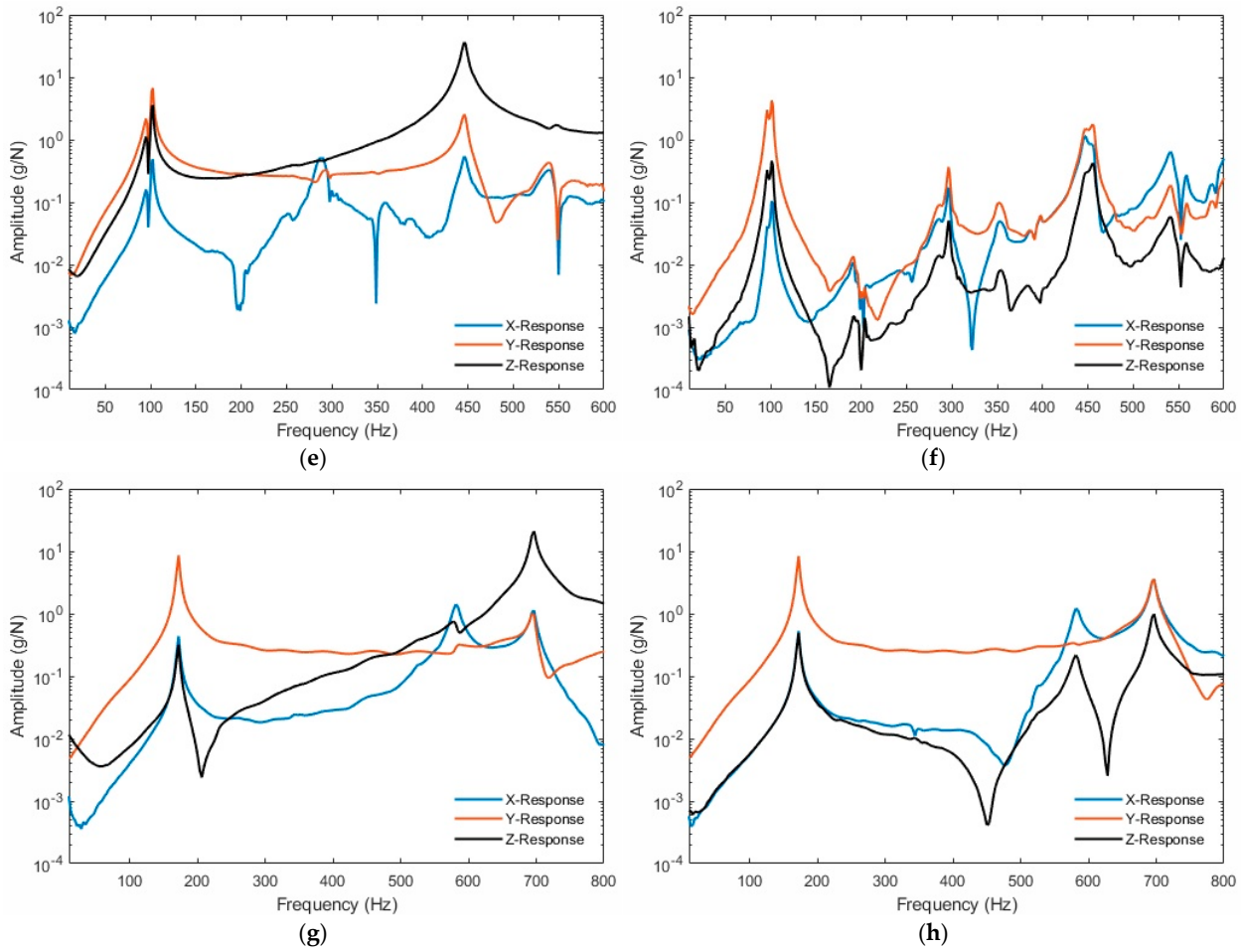

Figure 4. Frequency response functions from impact tests from (**a**) 0.5″ cut top, (**b**) 0.5″ cut side, (**c**) 0.25″ cut top, (**d**) 0.25″ cut side, (**e**) 0.1″ cut top, (**f**) 0.1″ cut side, (**g**) no-cut top, and (**h**) no-cut side box assembly systems.

Looking at Tables 3 and 4, it can be determined what direction the box assembly systems are moving by referencing the coordinate system in the upper left corner. In doing so, they can be compared to the results shown in Figure 4. Table 3 shows that mode 1, both (a) and (b) among all the cut systems, should be moving primarily in the Y-direction for both top and side accelerometers. Consequently, it is expected that the response will be highest in the Y-direction for this mode. Looking at the results from the impact tests, depicted in Figure 4, both the top and side accelerometers show the response to be highest in the Y-direction, as is expected from the FEA. Looking at mode 2 and continuing to focus on all the systems with a cut, it can be observed that the dynamical movement primarily occurs in the X-direction, specifically through the top accelerometer in the (a) modes. A small peak is seen in each response, near 300 Hz. This peak shows a high response in the X-direction, which again is predicted from the FEA. Finally, looking at mode 3 in Table 4, the dynamical movement occurs primarily in the Z-direction, specifically in the top accelerometer. Referencing the impact testing results from the top accelerometers, shown is a consistently high response in the Z-direction around 475 Hz, which again is expected from the FEA.

The impact testing results for the no central cut box assembly configuration are shown in Figure 4g,h. The dynamics of this system are slightly different than those with a central cut, but the basic characteristics are still comparable. Once again, the first mode is dominated by a moving displacement in the Y-direction, and this is shown in the response from both the top and side accelerometer. As for the second mode, which is near 600 Hz,

the X-direction in both accelerometers is the most dominant, as shown in Figure 4g,h. On the other hand, for mode 3 (around 700 Hz), it is clear that the top accelerometer is mostly moving in the Z-direction and the side accelerometer has more oscillations in the Y-direction.

Comparing the dominant frequencies found through FEA in Table 5 to those found from the impact testing, depicted in Table 6, it is clear that a similar trend is observed when the central cut is varied. Once again, as expected, the no-cut system shows the highest dominant frequencies of all the systems. Again, this is because the system lacks a cut, making it stiffer. Something that would previously seem unexpected is the presence of higher frequencies for the 0.25″ system. It is not surprising in this work since this agrees with the FEA conducted in Table 5, and higher frequencies are seen for the 0.25″ cut system among all the other box assembly systems with a cut when accelerometers are present. The exact reasoning for this is unknown, but this behavior may be due to the additional loading mass of the accelerometer and how it influences the overall dynamics of the box assembly system. To understand why the dominant frequency may be experiencing these changes, we can refer to a simplified linear expression to compute these frequencies. This is carried out by dividing the stiffness of the system (k) by the mass of the system (m) and square rooting that value. By altering the cut width, we are reducing the mass of the system and the stiffness. The rate at which these change with respect to the cut width will ultimately determine the dominant frequencies observed. It is also worth noting that comparing the 0.5″ and 0.1″ cut widths shows a similar decrease as seen in the FEA.

Table 6. Dominant frequencies for each cut system found through impact testing.

	Mode 1 (Hz)		Mode 2 (Hz)		Mode 3 (Hz)	
	(a)	**(b)**	**(a)**	**(b)**	**(a)**	**(b)**
0.5″	97.656	103.906	296.875	305.469	467.188	489.062
0.25″	104.69	106.25	318.75	326.562	475.00	495.312
0.1″	96.25	101.25	286.25	296.25	447.50	455.00
No	171.88		581.25		696.875	

Comparing the dominant frequencies obtained experimentally (Table 6) to their computational (Table 5) counterpart, it is noted that across all the box assembly systems, lower dominant frequencies are observed experimentally compared to the FEA counterpart. This is due to the ideal conditions considered when conducting the computational analysis. As previously described in the methodology, restrictions are imposed on the translation in X-, Y-, and Z-directions within the holes of the BA's base plate. This will result in a very stiff system, so the frequencies are expected to be greater. To create a more representative model, each bolted joint would require extensive modeling which is outside the scope of this study. In reality, as near-ideal conditions as possible are used, but are never quite as perfect as an FEA scenario. Though the computational dominant frequencies are higher, the trends are qualitatively similar. Confidence in the results is assured due to similar mode shapes being observed through both the simulated and experimental values in the plot.

4.2. Impacts of the Central Cut Width on the Dynamics of the Box Assembly Structure: Random Vibration Testing

The second set of experiments performed on the box assembly systems is through random vibration tests. The setup was described previously in Section 2. Random testing gives a qualitative understanding of the dynamics of each system. A pseudorandom excitation is considered for this testing because of the interest in the nonlinear characteristics that can be determined by incrementally increasing the excitation levels. Thirty averages were performed in each test to ensure that the data shown in the power spectral density

(PSD) plots could be clearly read. Pseudorandom excitation gives a constant amplitude and periodicity in the sample interval, which allows for sensitivity to nonlinearities. The trends that can be observed are done so by dividing the output response by the input signal [37]. Through this testing, an analysis of how the system reacts over a range of frequencies under various excitation levels is observed. Specialty trends are to be expected, varying between nonlinear softening, hardening, and/or damping. These findings will be investigated and discussed later in this study.

4.2.1. Random Vibration Testing Investigating Results from the Y-Direction

Figure 5 shows the PSD results from all the central cut widths for four different input levels of excitations. Both top and side Y-direction accelerometer results are plotted in Figure 5a,c,e,g and Figure 5b,d,f,h, respectively. Inspecting these subfigures, it can be observed that all the experimental results show similar trends for the different central cut configurations. Again, the focus will be on modes 1(b) and modes 3(b) from Tables 3 and 4. Notice that the highest responses are from these modes, since this is the direction that has the largest dynamical movement in the Y-direction for the side accelerometer. These modes peak at approximately 105–120 Hz and 500–550 Hz, respectively, depending on the cut width being observed. From the plotted graphs in Figure 5b,d,f for the various central cut widths, it can be observed that an increase in the input excitation is accompanied by a decrease in the dominant frequency near the first and third modes. This is a characteristic of the presence of a nonlinear softening in the box assembly configurations with cuts. An example of a nonlinear softening trend is seen in Figure 5b.

As for the no central cut configuration, shown in Figure 5g,h, the experimental results are similar for both the side and top accelerometers in the Y-direction. Further, although the data appears noisier near the first (≈175 Hz) and third (≈725 Hz) modes of vibration, the second mode of vibration (around 580 Hz) shows the existence of a slight nonlinear softening behavior.

Table 7 shows the tabulated dominant frequencies found through random vibration testing using the side accelerometer in the Y-direction. The focus primarily being on the side accelerometer is due to the data showing a better quality of results than the top one in this direction. Here, it is easier to see the nonlinear softening trend present. Notice how, as the excitation increases from 10^{-7} V^2/Hz to 10^{-4} V^2/Hz, the dominant frequencies decrease. Furthermore, if the systems with central cuts are compared, a linear softening trend can be observed. As the cut width decreases, the dominant frequencies also decrease. A percent change is also calculated to determine the difference between the frequency of the lowest excitation (10^{-7} V^2/Hz) and the highest excitation (10^{-4} V^2/Hz). Just focusing on the systems with a cut, the highest percent change in these dominant frequencies is the 0.1” cut, where a 2.41% change is seen in the first mode and a 3.04% change is seen in the third mode. It is also worth noting that the peak frequencies seen in the 0.25” cut system during the FEA and impact testing are not seen here, possibly due to the experimental setup used for random vibration, and hence the possible added stiffness by the stinger to the overall system or the interaction between the system and the slip table setup. Something else to discuss is the nonlinear softening trend seen in the no-cut system. This system shows a much stronger trend than what is seen in the cut systems, with a softening of 3.49% in the first mode and a 4.18% softening in the third mode.

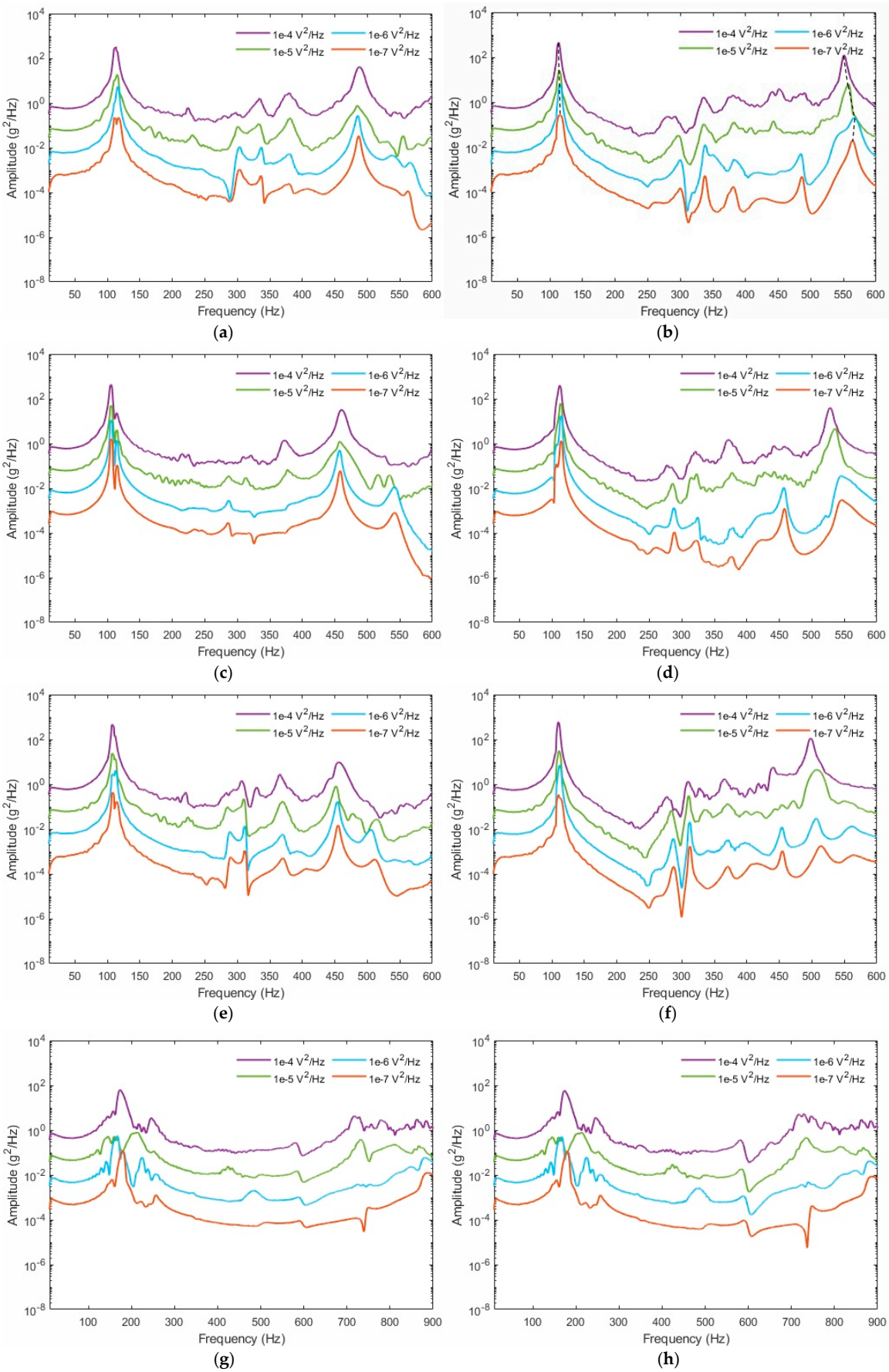

Figure 5. PSD results from all cut widths in Y-direction: (**a**) 0.5″ cut top, (**b**) 0.5″ cut side, (**c**) 0.25″ cut top, (**d**) 0.25″ cut side, (**e**) 0.1″ top, (**f**) 0.1″ side, (**g**) no cut top, and (**h**) no cut side.

Table 7. Dominant frequencies from modes 1(b) and 3(b) found through random vibration testing from side accelerometer.

	0.5″ Cut (Hz)		0.25″ Cut (Hz)		0.1″ Cut (Hz)		No Cut (Hz)	
	Mode 1	**Mode 3**	**Mode 1**	**Mode 3**	**Mode 1**	**Mode 3**	**Mode 1**	**Mode 3**
$1e^{-7}$ V^2/Hz	116.406	564.062	114.453	545.312	113.281	513.281	179.297	747.656
$1e^{-6}$ V^2/Hz	115.625	566.406	114.062	544.141	112.109	508.203	167.188	738.281
$1e^{-5}$ V^2/Hz	115.234	557.812	114.062	536.328	112.109	508.203	159.766	732.422
$1e^{-4}$ V^2/Hz	114.062	550.781	112.891	528.906	110.547	497.656	173.047	716.406
% Change	2.01%	2.35%	1.36%	3.01%	2.41%	3.04%	3.49%	4.18%

Shown in Figure 6 are the output/input plots found for the various box assembly systems from the Y-direction of the top and side accelerometers. Comparing all the systems with a cut, similar trends are observed. Once again, the results are compared to the mode shapes found in Tables 3 and 4. For example, immediately seen are the highest responses at approximately 110–120 Hz in all the systems with a cut. This is expected since mode 1(b) in Table 3 are moving primarily in the Y-direction on the side with the accelerometer, as shown in Figure 6a. No other mode is expected to have that high displacement since no other mode is moving as much in that direction. The next mode of particular interest is mode 3, particularly mode 3(b) of all the central cut systems since that side is moving with the accelerometer. Though very slight, the side accelerometer is moving in the Y-direction, as shown in Figure 7b. Here, in the third mode of the system around 500–550 Hz, a nonlinear damping trend is observed. This trend is present in the lower modes, but not as evident as it is in the higher modes of interest.

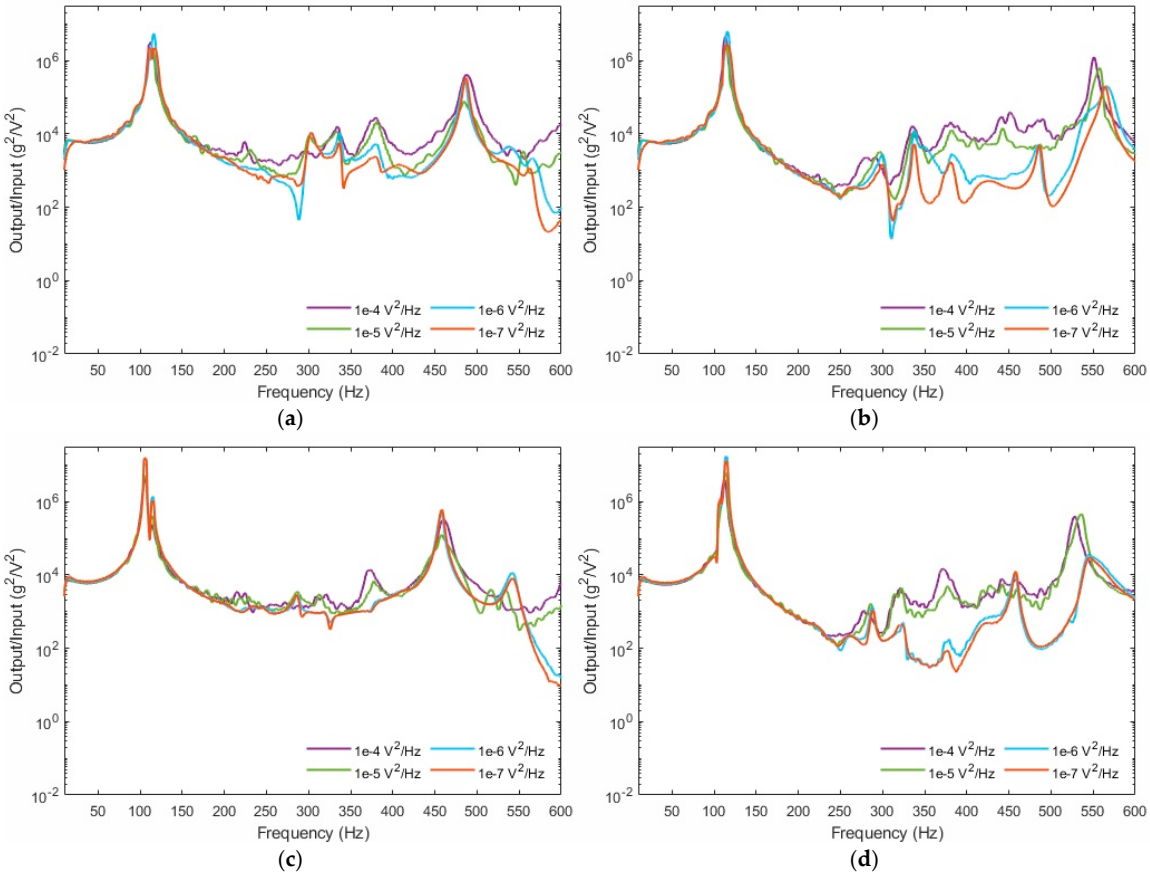

Figure 6. *Cont.*

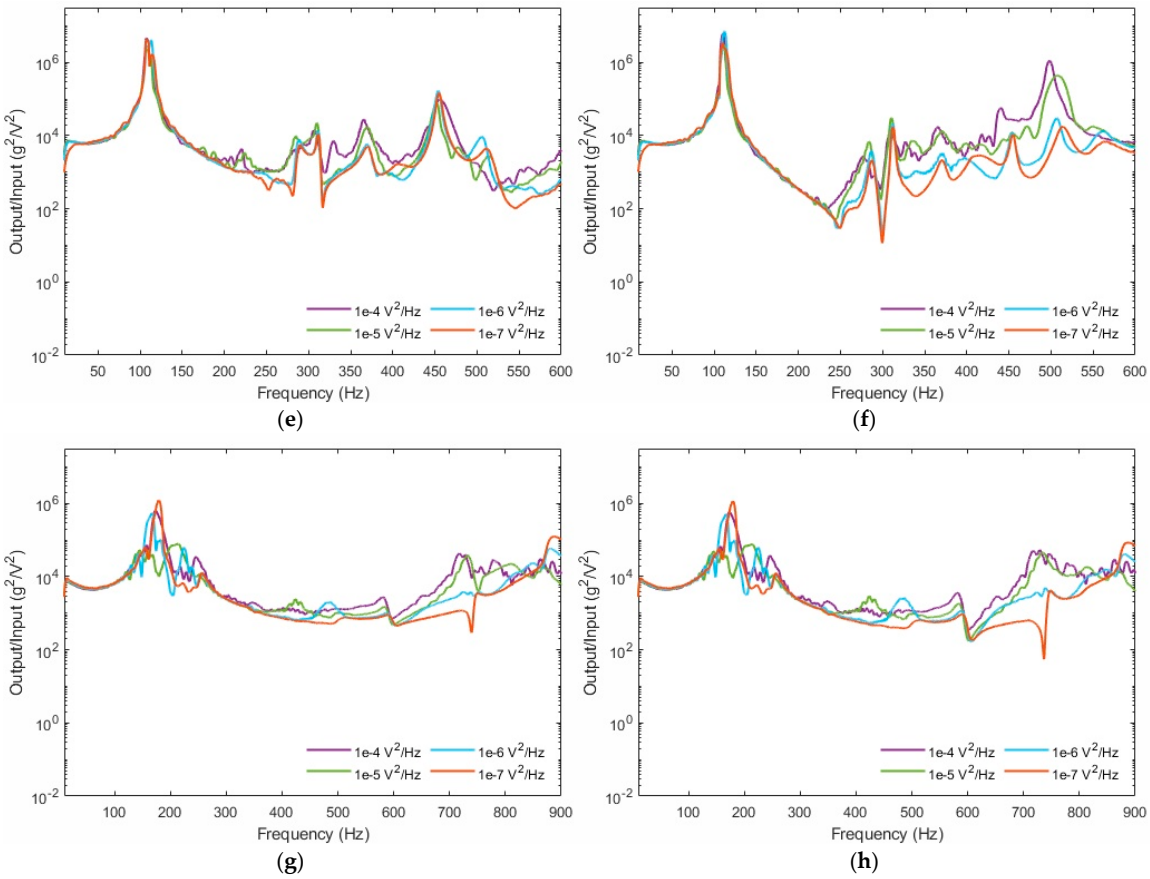

Figure 6. Output/input plots from the random vibration tests for the (**a**) 0.5″ cut top, (**b**) 0.5″ cut side (**c**) 0.25″ cut top, (**d**) 0.25″ cut side, (**e**) 0.1″ cut top, (**f**) 0.1″ cut side, (**g**) no-cut top, and (**h**) no-cut side box assembly systems from the Y-direction.

The no-cut system shows similar behaviors to the cut systems but is worth discussing separately from those modes with a cut. Observe Figure 6g,h, where the output/input plot of the no-cut system is demonstrated. Again, a dominant peak frequency is seen around 175 Hz, where a high response from the side accelerometer is expected due to considerable movement from the system in that direction. This movement can be observed in Table 3 of mode 1 in the no-cut system. Furthermore, high responses are again in the higher mode, not as high as mode 1 since the motion is not as strong compared to mode 1, but still obviously present. See Figure 6h for the motion of the no-cut system in this direction. Here, a nonlinear damping trend can be observed, as each excitation differs from one another. This is not seen on the systems with a cut. The trend becomes more and more apparent for higher frequencies, and it is very evident in mode 3 around 750 Hz. Similar results are shown in both the top and side accelerometers in all the systems. The main difference between the accelerometers is the presence of nonlinear damping in early modes, shown almost instantly in the side accelerometer versus the top accelerometer.

4.2.2. Random Vibration Testing Investigating Results from the X-Direction

A similar investigation is conducted in Figure 7 looking at both accelerometers, but this time in the X-direction. Little to no nonlinearities are shown, since the system is being excited in the Y-direction, not the X-direction, and only the second mode-related cases have been influenced in the X-direction. Though trends involving dominant frequencies and mode peaks are still similar, trends of nonlinearities are not as relevant in these data as were in the Y-direction. Some nonlinearities, though, can still be examined when looking at the second vibratory mode in all the cut width results.

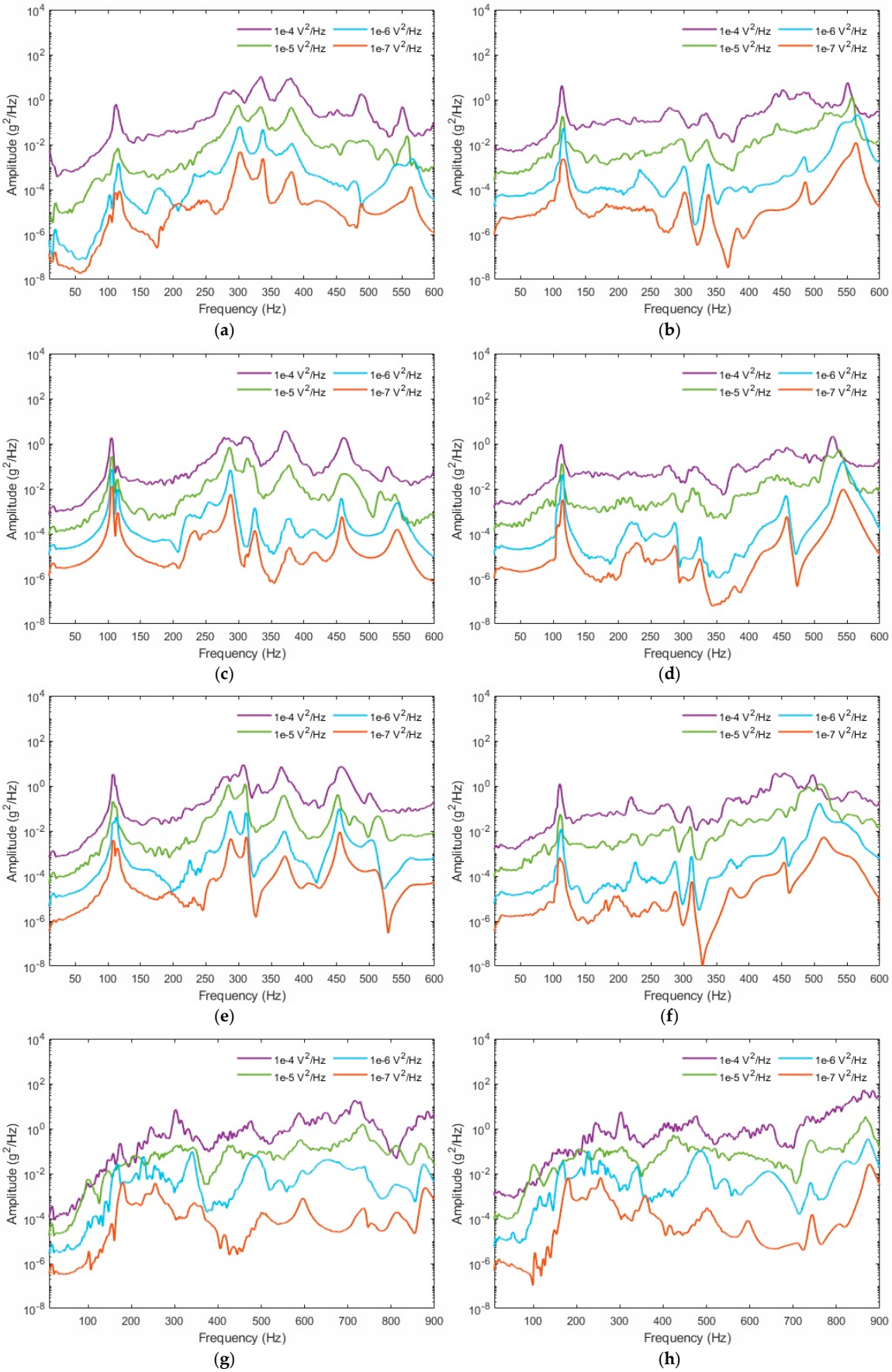

Figure 7. PSD results from all cut widths in X-direction: (**a**) 0.5″ cut top, (**b**) 0.5″ cut side, (**c**) 0.25″ cut top, (**d**) 0.25″ cut side, (**e**) 0.1″ top, (**f**) 0.1″ side, (**g**) no cut top, and (**h**) no cut side.

Table 8 shows the resonant peaks for each system from mode 2. Notice the nonlinear softening trend taking place. As the excitation increases, the dominant frequencies decrease in all the cases. This nonlinear softening is strongest in the 0.25″ cut system, having a 3.67% change from the lowest excitation to the highest excitation. An interesting trend is the no-cut softening being weaker than what was seen in Table 7. The no-cut case has a nonlinear softening trend of only 1.57%, as compared to the 3.49% and 4.18% softening trends for modes 1 and 3, respectively. The nonlinear softening trend comparing the cut widths is once again prevalent here, but is stronger in the higher excitations. It should be mentioned that a focus has been paid to similar peak frequencies (named as mode in this section) for all the cut cases, so the comparative study between all the central cut configurations can be discussed in the random vibration section.

Table 8. Dominant frequencies from mode 2 found through random vibration testing from side X accelerometer.

	0.5″ Cut (Hz)	0.25″ Cut (Hz)	0.1″ Cut (Hz)	No Cut (Hz)
	Mode 2	Mode 2	Mode 2	Mode 2
$1e^{-7}$ V^2/Hz	301.953	287.5	287.5	596.094
$1e^{-6}$ V^2/Hz	301.562	286.719	287.109	593.75
$1e^{-5}$ V^2/Hz	300	285.938	284.375	590.625
$1e^{-4}$ V^2/Hz	292.188	276.953	277.734	586.719
% Change	3.23%	3.67%	3.40%	1.57%

Continuing the explanation for why little is shown in the directions other than the Y-direction, the top-down views of the box assemblies from the computational analysis are shown in Figure 8. Notice how little the accelerometers are moving in the X-direction and Z-direction. This explains why nonlinearities cannot be observed when analyzing the data. A lot of motion is shown in the Y-direction on the side accelerometers, especially in mode 1. Though not a lot of motion is shown in mode 3, the accelerometer is still moving slightly in that direction.

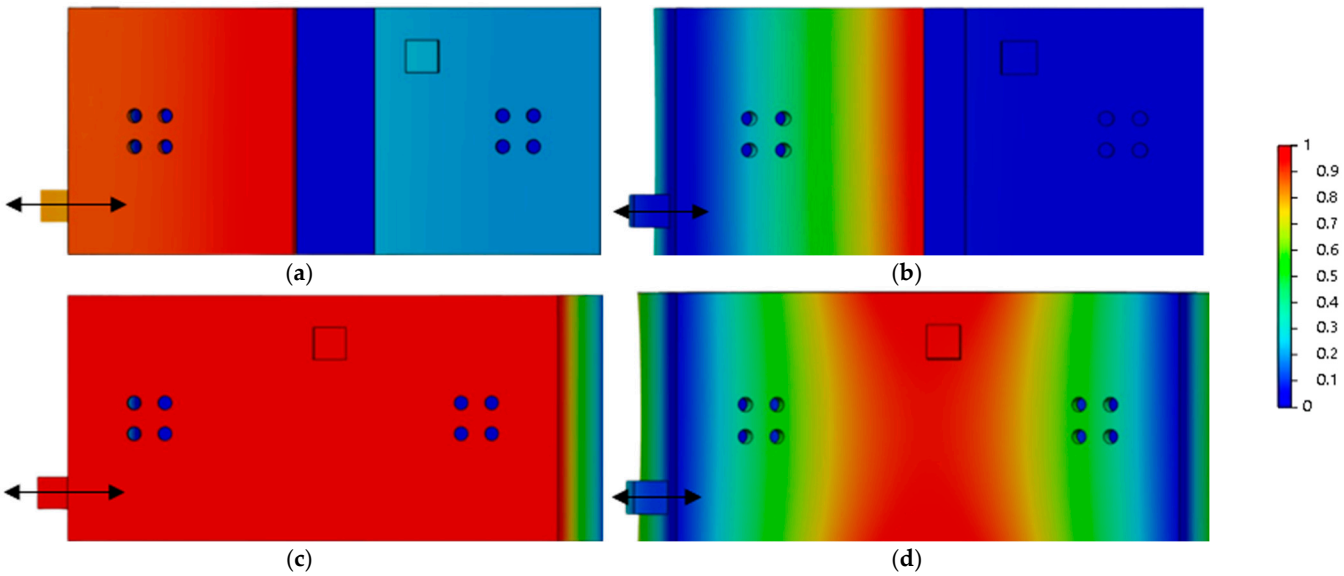

Figure 8. Top-down view of 0.5″ cut (**a**) mode 1b and (**b**) mode 3b and no cut (**c**) mode 1 and (**d**) mode 3 including a normalized color bar.

4.2.3. Discussion of the Impacts of the Central Cut Width on the Dynamics of the Box Assembly Structure Using Random Vibration Testing

The random vibration testing section showed various results that helped determine the influence altering the cut width would have on the box assembly system. Figure 9 gives an in-depth view of how an input uncertainty in the central cut width may affect the dynamics of the box assembly system. This figure shows the results of all the cut widths on a single plot using two different accelerometers to clearly examine the impact the central cut has in different directions. Each of these data sets was taken from the $1e^{-4}$ V^2/Hz excitation case, since this is the highest excitation and gives the clearest results. Inspecting the PSD plots in Figure 9, it is clear that an increase in the central cut width is accompanied by an increase in the dominant frequencies of the box assembly system for all the modes of vibration under investigation. In addition to the change in the dominant frequencies, there is variability in the amplitudes of the box assembly's oscillations for both accelerometers. This change in the amplitude is more important at higher frequencies. To this end, it is important to accurately measure the central cut width in order to precisely determine the dominant frequencies and amplitudes of the system.

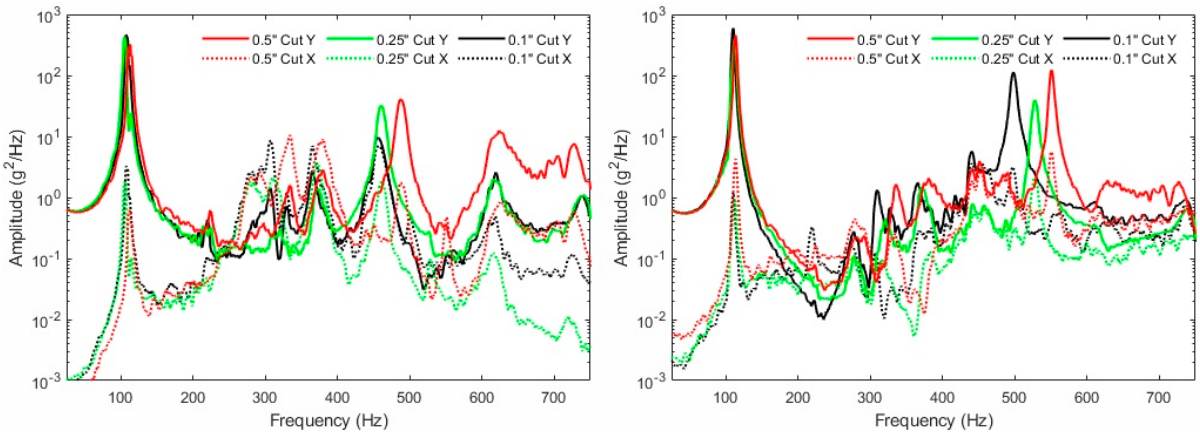

Figure 9. A comparison of cut widths and response directions from the (**a**) top accelerometer and (**b**) side accelerometer.

Further, from the plots shown in Figure 9, it is noticed that the Y-direction is consistently larger in amplitude versus the X-direction for the first dominant peak. Referring to the FEA mode shapes in Table 3, it can be observed the first mode moves primarily in the Y-direction. Table 3 also shows the second mode, where the top accelerometer is moving primarily in the X-direction. By looking at Figure 9, especially the top accelerometer, the X-direction data are seen to better demonstrate the dominant frequency. Finally, since mode 3 can be observed in Table 4 to be moving primarily in the Y-direction, Figure 9 shows the third peak to be dominant with the Y response data.

What is seen in Figure 9 agrees with the impact testing data as well, as depicted in Figure 4. There, the first peak is dominant in the Y-direction while the second peak is dominant in the X-direction. Similar trends are observed in the random testing data, giving confidence in the results of each investigation. A trend that was seen in the impact data and not seen here in the random vibration section is the peak frequencies of the 0.25" cut system. Both the FEA and impact data showed a trend of peak frequencies among all the cut widths for that system. Here, the trend was not observed. This could be due to a number of uncertainties, one of which is the stiffness the stinger may add to the system. Because of this added stiffness, the 0.25" cut box assembly reacts differently than one would expect. The FEA and the impact tests did not utilize a stinger. Another potential uncertainty is the

influence of asymmetry the system has. An interaction may occur between modes since they are very close to one another in terms of frequency. These modes might mesh together and influence one another, causing results not previously seen.

4.3. Influence of the Cut Width on the Dynamics of the Box Assembly Structure: Harmonic Vibration Testing

During harmonic vibration testing, stepped sine excitation was applied to each system with a hold time of ten seconds. The system was excited near resonance for the first mode. The goal was to quantify the presence of nonlinearities that were observed in random vibration testing, whether a nonlinear softening trend was seen or not. In addition, a quantitative nonlinear damping analysis was performed near the first mode of vibration for all the configurations. As a result, these data are very important in determining the validation of trends already seen in the system. Both Y- and X-directions are investigated in this section for both side and top accelerometers.

4.3.1. Harmonic Vibration Testing Investigating Results from the Y-Direction

Figure 9 depicts the results of the Y-direction harmonic testing performed on each box assembly system. The experimental setup can be found in Figure 3. Harmonic testing gives a quantitative analysis of the system's dynamics. Each box assembly system was excited at four different input levels of excitation, namely, 50 mV, 100 mV, 125 mV, and 150 mV. The harmonic tests were focused around the first mode of vibration in order to effectively characterize the dynamical properties of these systems and how the possible uncertainty or change in the central cut width influences the system's response. It follows from the plots in Figure 9 that a nonlinear softening trend is present in each system, showing similar results to the random vibration tests. Again, as the excitation level increases, the resonant frequency decreases. It should be noticed that two resonant frequencies are present in each system, which again confirms the asymmetry seen earlier in the FEA and impact tests due to the placement of the accelerometers.

Another incident to note is the difference in linear behaviors between the two peaks. The left peak in all the plots shown is more linear than the second peak for all the central cut widths of 0.5", 0.25", and 0.1". According to the simulations, the first peak is associated with mode 1(a), where the top accelerometer is generally more influenced, while the second peak is associated with mode 1(b), where the side accelerometer is generally moving more. This comparative oscillating behavior is particularly true for the 0.5" configuration. It should be mentioned that the placement of the accelerometers may change the overall behavior of the system even with a little uncertainty [3].

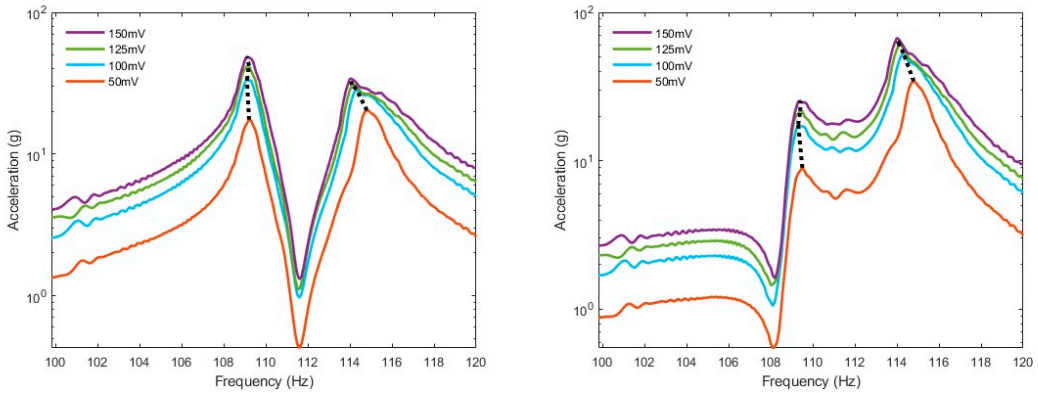

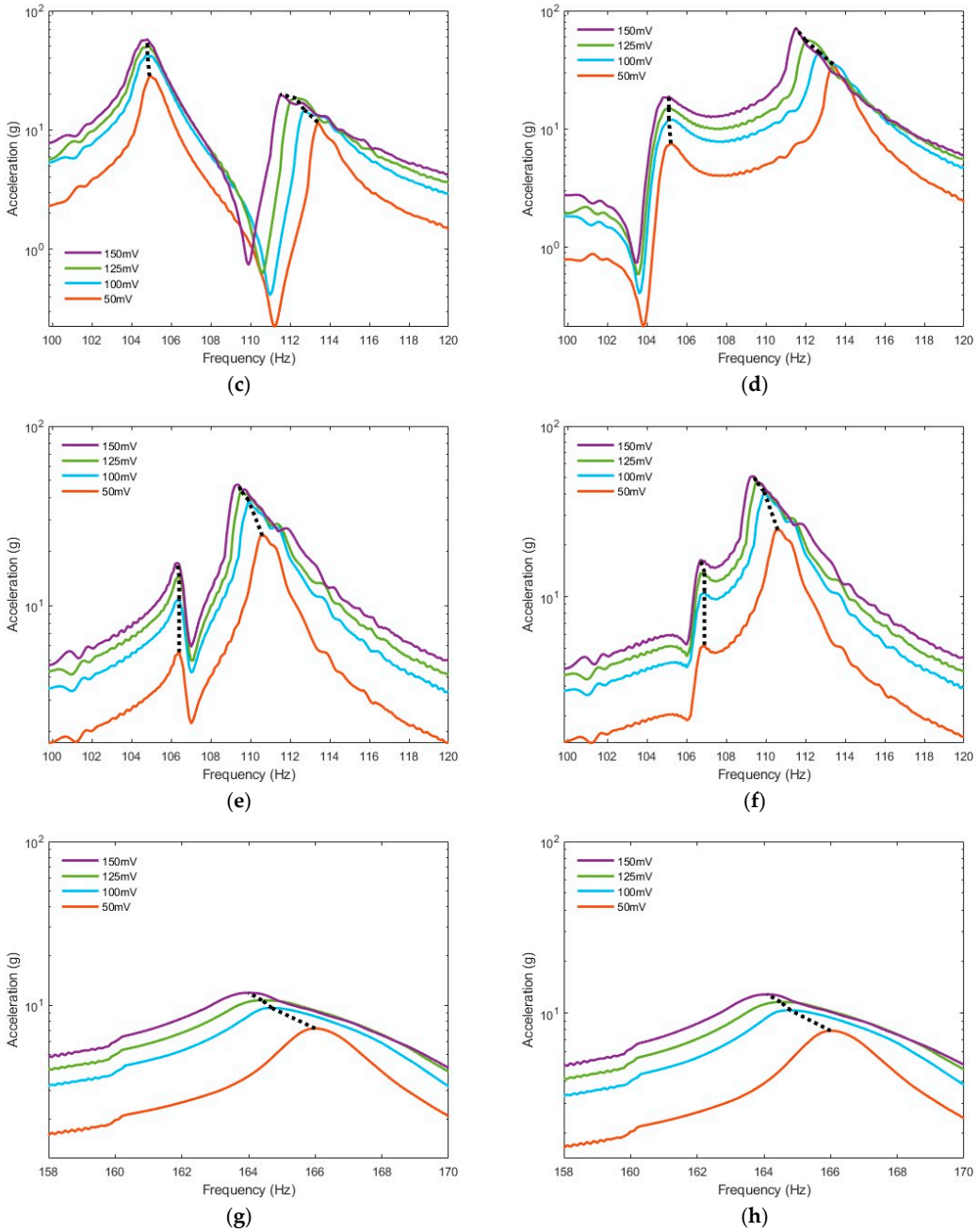

Figure 9. FRF harmonic testing results in Y-direction from (**a**) 0.5″ cut top, (**b**) 0.5″ cut side, (**c**) 0.25″ cut top, (**d**) 0.25″ cut side, (**e**) 0.1″ cut top, (**f**) 0.1″ cut side, (**g**) no cut top, and (**h**) no cut side showing backbone trends among each test.

Inspecting the frequency response curves of both the top and side accelerometers in Figure 9, it is noted that the oscillating amplitudes for the first and second resonant peaks are higher for the top and side accelerometers, respectively, for both the 0.5″ and 0.25″ central cut width scenarios. On the other hand, the 0.1″ central cut width configuration shows that the oscillating acceleration amplitude of the second resonant peak is higher than the first resonant frequency counterpart for both the top and side accelerometers, as shown in Figure 9e,f. This means that the side accelerometer's motion is more significant than the top accelerometer's one. As for the side accelerometer's amplitudes, they are always higher for their corresponding mode 1(b) for all the width cut configurations, as presented in Figure 9b,d,f. It should be mentioned that an anti-resonance behavior takes place between the two resonant peaks, and this is particularly true for the top accelerometer's results.

Table 9 depicts the harmonic vibration results in a tabulated view, showing the resonant frequencies for each cut from the side accelerometer. Similarly to the results found in Table 7, only the side accelerometer is considered, since it gives the best quality results in this direction. Here, the cut widths can be more easily compared to one another. A nonlinear softening trend is observed in all the cut widths, including the no-cut system. When comparing the cut systems to one another, it can be observed that a linear softening trend can again be observed since, as the cut width decreases, the dominant frequencies also decrease.

Table 9. Resonant frequencies from left and right peaks of mode 1 found through harmonic vibration testing from side accelerometer.

	0.5″ Cut (Hz)		0.25″ Cut (Hz)		0.1″ Cut (Hz)		No Cut (Hz)
	L Peak	R Peak	L Peak	R Peak	L Peak	R Peak	Peak
50 mV	109.5	114.8	105.2	113.4	106.9	110.6	166.0
100 mV	109.3	114.3	105.1	112.7	106.9	109.9	164.8
125 mV	109.4	114.1	105.1	112	106.9	109.5	164.5
150 mV	109.4	114	105.1	111.5	106.7	109.4	164.1
% Change	0.09%	0.70%	0.10%	1.68%	0.19%	1.08%	1.14%

In addition to the difference in the nonlinear softening between the cut configurations, as indicated in Table 9, the difference between the two resonant frequencies changes too. Indeed, for the lowest input excitation scenario, the difference in resonant frequencies for the 0.5″, 0.25″, and 0.1″ change to 5.3 Hz, 8.2 Hz, and 3.7 Hz, respectively. This result shows the interaction between the two modes and the possible coupling between them and how it influences the broadband region and the amplitudes of the oscillations.

The output/input frequency response curves plotted in Figure 10 continue to show what was discussed in the random vibration section of this study. Again, the results show a nonlinear damping trend present, especially in the second peak in both the top and side accelerometers. An interesting trend is shown in Figure 10c,d for the 0.25″ cut BA system. Looking at the first group of peaks for this system, a slight nonlinear damping trend can be seen. Notice that the peaks do not stack uniformly over one another as the peaks for the other systems do. It follows from the plots in Figure 10 that an increase in the input excitation is accompanied by a decrease in the output/input amplitude, which is a characteristic of the presence of higher damping in the system at higher excitation levels. This may be due to the friction in the base of the box assembly.

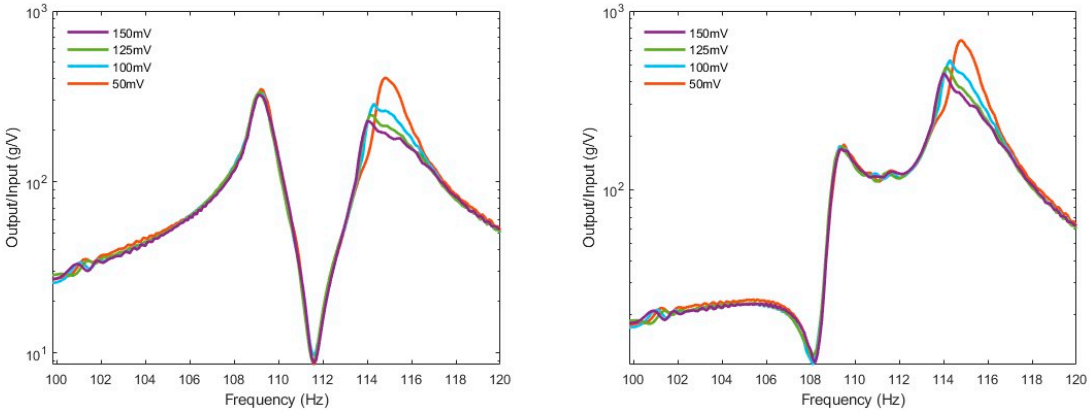

Figure 10. *Cont.*

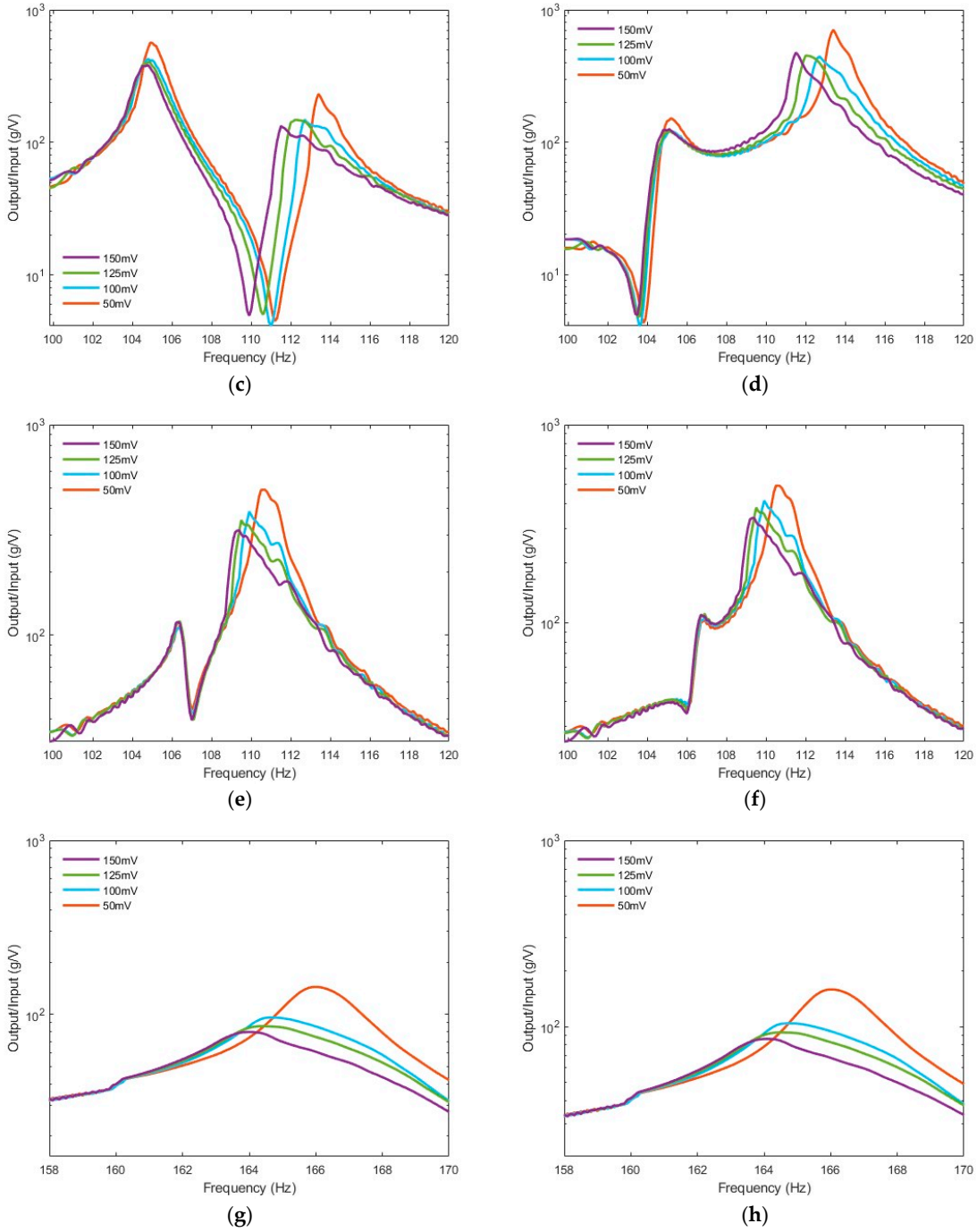

Figure 10. Output/input harmonic testing results in Y-direction from (**a**) 0.5″ cut top, (**b**) 0.5″ cut side, (**c**) 0.25″ cut top, (**d**) 0.25″ cut side, (**e**) 0.1″ cut top, (**f**) 0.1″ cut side, (**g**) no cut top, and (**h**) no cut side.

In order to show the damping present in the systems, Table 10 is generated using the output/input plots from the side accelerometer. This table gives a better analysis of the damping trends seen in each system. The right peak consistently shows greater damping than the left peak, and this is true across all the systems. It is also worth noting that a consistent damping trend can be observed when comparing the cut systems, where the 0.5″ cut system has the highest percent change, decreasing to the 0.25″ cut system and then again decreasing to the 0.1″ cut system, which has the lowest percent change. It is important to note that the percent change is taken from the lowest and highest excitation levels. The no-cut system has the highest damping percent change among all the systems, with a percent change of 45.76%.

Table 10. Amplitude found using harmonic vibration testing from the output/input plots of the side accelerometer.

	0.5″ Cut (g/V)		0.25″ Cut (g/V)		0.1″ Cut (g/V)		No Cut (g/V)
	L Peak	R Peak	L Peak	R Peak	L Peak	R Peak	Peak
50 mV	179.20	685.33	151.53	706.63	104.27	492.21	158.22
100 mV	175.41	531.31	120.06	444.04	107.73	414.06	104.00
125 mV	173.51	482.87	119.72	451.21	111.22	381.48	92.976
150 mV	168.59	447.98	125.33	474.42	106.68	338.04	85.813
% Change	5.92%	34.63%	17.24%	32.86%	-2.31%	31.32%	45.76%

Some uncertainties in the experimental data may exist for the data shown in Figure 10, explaining why some irregularities could be observed. Figure 11 shows the response near resonance for the 150 mV excitation case for the 0.5″ cut system in the Y-direction. Notice that the response is not nearly as sinusoidal as one would expect. Further, it should be noted how the amplitude decreases as the frequency increases past resonance.

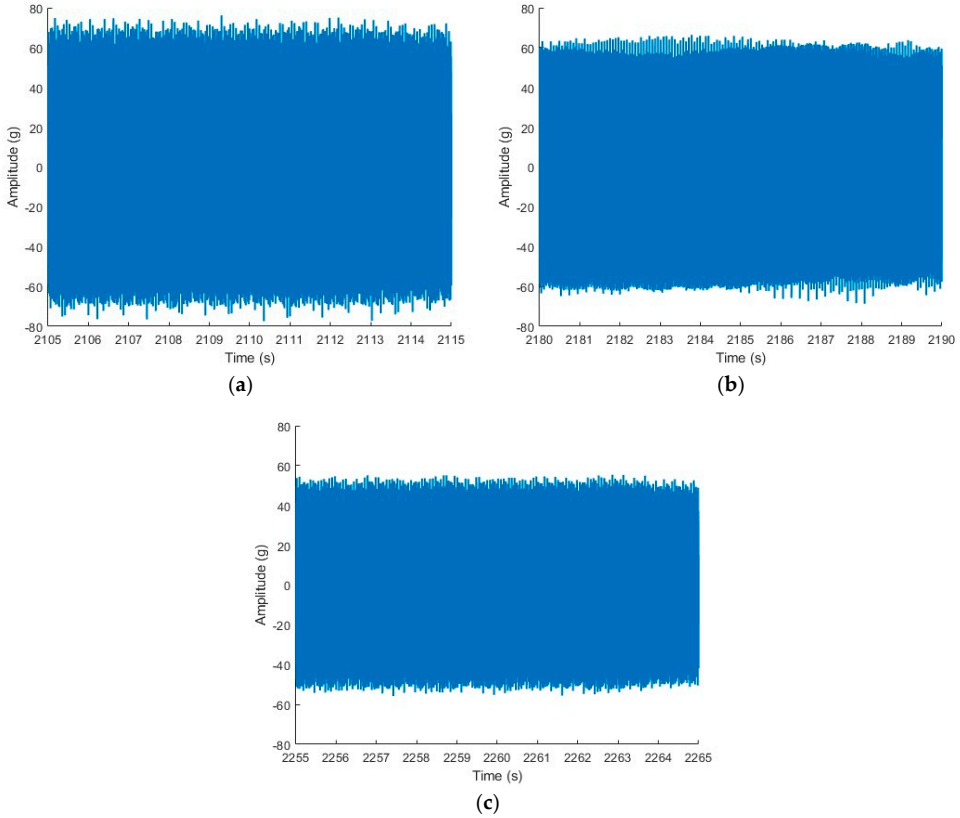

Figure 11. Time history of the 0.5″ cut case near resonance from the side accelerometer at 150 mV excitation, showing (**a**) 114 Hz (resonance), (**b**) 114.5 Hz, and (**c**) 115 Hz.

4.3.2. Harmonic Vibration Testing Investigating Results from the X-Direction

When comparing the Y-direction harmonic testing results to the X-direction counterpart, it is shown how difficult it is to observe the present nonlinearities in each system due to the dominance of the Y oscillation for the first modes of vibration. This can be seen in the frequency response curves in Figure 12. Each system is seen to have mode coupling as well with the poor quality of data shown. It can also be shown how low the amplitudes of oscillation will be when gathering data from this direction. Previously, the Y-direction showed an amplitude nearing almost 60 g's. Here, in the X-direction, the amplitude is almost reaching only 6 g's.

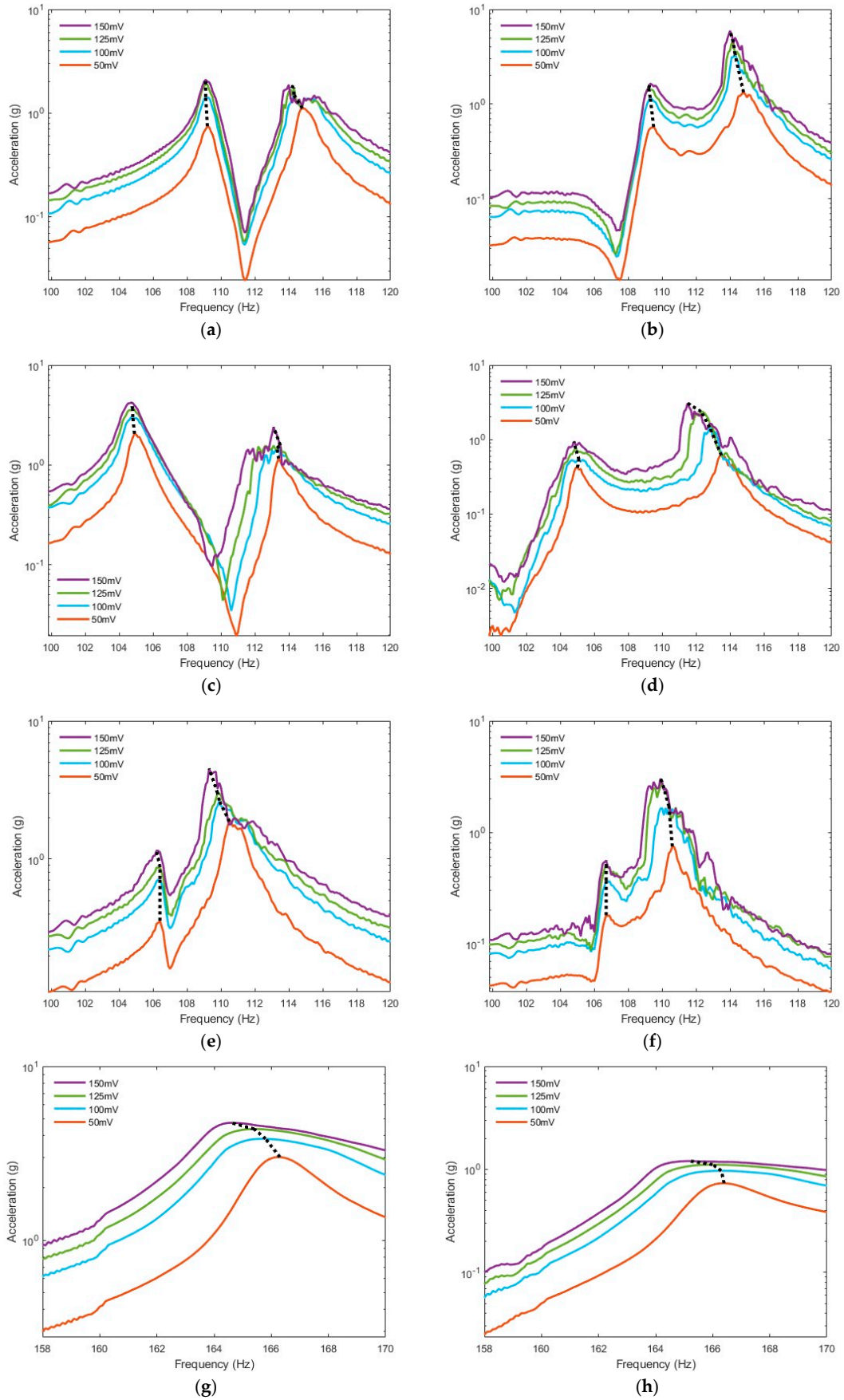

Figure 12. FRF harmonic testing results in X-direction from (**a**) 0.5″ cut top, (**b**) 0.5″ cut side, (**c**) 0.25″ cut top, (**d**) 0.25″ cut side, (**e**) 0.1″ cut top, (**f**) 0.1″ cut side, (**g**) no cut top, and (**h**) no cut side showing backbone trends among each test.

The tabulated dominant frequencies can be seen in Table 11. The top accelerometer is chosen for this analysis into the first mode of vibration. A nonlinear softening trend can be observed in all the test results. Again, notice how a softening trend occurs when comparing peaks between one another. As the cut width decreases, so do the dominant frequencies. This trend is true for both the left and right peaks. The system with the highest nonlinear softening is the 0.1″ peak, primarily in the right peak with a percent change value of 1.09%. This value is very similar to what is seen in Table 9.

Table 11. Tabulated dominant frequencies from left and right peaks of mode 1 found through harmonic vibration testing from top accelerometer.

	0.5″ Cut (Hz)		0.25″ Cut (Hz)		0.1″ Cut (Hz)		No Cut (Hz)
	L Peak	R Peak	L Peak	R Peak	L Peak	R Peak	Peak
50 mV	109.2	114.8	104.9	113.4	106.4	110.5	166.3
100 mV	109.1	114.3	104.8	113.3	106.4	109.9	165.8
125 mV	109.1	114.3	104.8	113.5	106.4	109.8	165.4
150 mV	109.1	114	104.7	113.1	106.2	109.3	164.6
% Change	0.09%	0.70%	0.19%	0.26%	0.19%	1.09%	1.02%

4.3.3. Discussion of the Impacts of the Central Cut Width on the Dynamics of the Box Assembly Structure Using Harmonic Vibration Testing

To further examine how the central cut width (1) impacts the existence and strength of nonlinearities and (2) influences the overall dynamics of the system in terms of the broadband regions, dominant frequencies, and amplitudes of oscillation, a deep investigation was performed for determining the quality factor of each box assembly configuration and a comparative study was carried out.

First, the quality factor for each accelerometer in the Y-direction was calculated and is depicted in Figure 13. Finding the quality factor allows for a better understanding of the nonlinear damping present in the system, particularly since the resonant frequency does not vary much in terms of percentage (less than 1.5%) for all the box assembly configurations, as shown in Table 11. As demonstrated earlier, the first modes 1(a) and 1(b) are mostly oscillating in the Y-direction. Further, the X-direction plots have a lot of variability due to the low levels of output amplitudes and the existence of several harmonics in the time history, so the main focus in this section is on the Y-direction results. The Y-direction quality factors' plots show that as the input excitation level increases, the quality factor decreases, as shown in Figure 13a,b. Since the quality factor is decreasing, the nonlinear trend has a higher effect as the excitation level increases. This means that the nonlinear damping has a higher effect as the excitation level increases. The outlier is the 0.25″ cut system in the side accelerometer Y plot. The trend is not the same as the others, instead decreasing and then increasing back at the higher excitations. One of the possible reasons is the presence of several harmonics in the time histories of the experimental data and hence, the possible uncertainties in the estimation of the amplitudes of oscillation at the quality factor's corresponding frequencies. It should be mentioned that efforts are made during experiments to ensure that all the joints are torqued the same before each test, but some uncertainties from preload loss could be credited to the damping in each system. It is possible that the torque of the joints changed throughout each test, which cannot be controlled without disturbing each experiment.

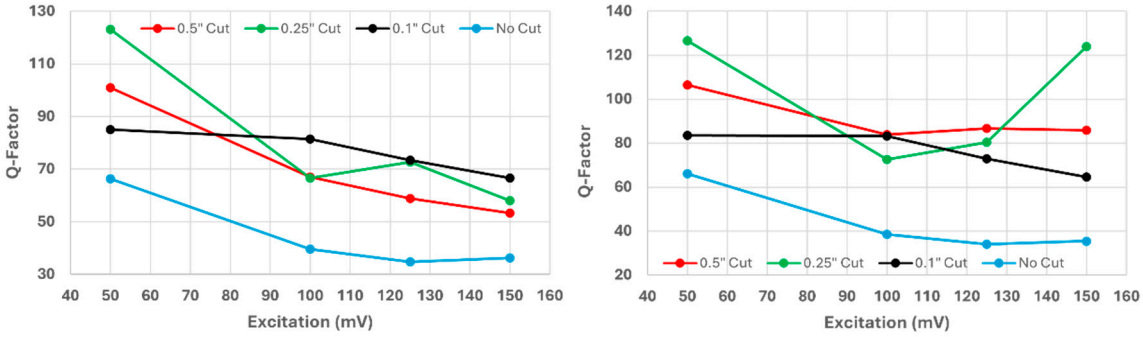

Figure 13. Quality factor plots for the (**a**) top Y and (**b**) side Y accelerometers.

Second, in order to directly explore the effects of the central cut width on the dynamical response of the box assembly, an investigation into individual cut widths comparing the input excitations was also conducted, as depicted in Figure 14. Inspecting this figure's plots, it is clear that a little change in the central cut width results in a significant variation in the box assembly's responses. In fact, a decrease in the central cut width results in a linear softening in the first modes of vibration, as shown in Table 9. In addition, the broadband range between the two resonant frequencies varies depending on the cut width. As for the amplitudes of oscillations and the coupling/interaction between the two modes, they are strongly dependent on the cut width.

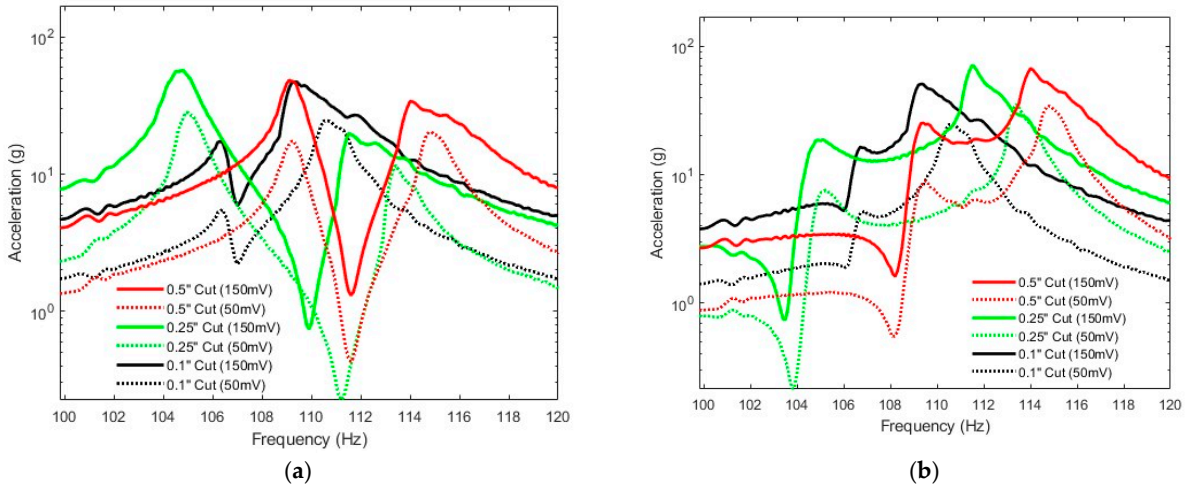

Figure 14. A comparison of excitation frequencies between cut widths for the Y-direction using the (**a**) top and (**b**) side accelerometers.

5. Conclusions

Little to no work in the literature has shown how the central cut width affects the characteristics of the box assembly of the BARC system. Both computational simulation and experimentation were performed on various box assembly structures with varying central cut widths to investigate the variability in the linear properties and nonlinear behaviors due to this possible geometric uncertainty. The finite element analysis performed on each system demonstrated asymmetry between each system where a cut exists and the no-cut system, particularly due to the presence of the accelerometer and the cut within the system. It was also observed that the system with the highest peak frequencies is the 0.25″ cut system, as shown in both the FEA and the impact data. Dominant frequencies between the 0.5″ cut and the 0.1″ cut systems were similar throughout all the testing. It was also determined that there is a strong nonlinear damping present in the higher modes

of each system, while a nonlinear softening trend is present in all the test results. These trends were observed in both the random and harmonic testing results. For brevity, not all the directions were shown in this study, particularly the results from the Z-direction accelerometers. When performing random and harmonic testing on the 0.25″ cut BA, the high frequencies were not observed as they were previously in the FEA and impact testing results. The significance of modeling the accelerometers and precisely measuring the central cut width due to any manufacturing or design uncertainties was clearly examined in this study. This little variation in the central cut width may change the dynamical responses and characteristics of the box assembly system.

Author Contributions: Conceptualization, A.A.; methodology, C.P., A.F., E.G., J.M. and A.A.; software, C.P., A.F., E.G. and J.M.; validation, C.P.; formal analysis, C.P. and A.A.; investigation, C.P., A.F., E.G., J.M. and A.A.; resources, A.A.; data curation, C.P.; writing—original draft, C.P.; writing—review and editing, A.F., E.G., J.M., and A.A.; visualization, C.P., A.F., E.G., J.M. and A.A.; supervision, A.A.; project administration, A.A.; funding acquisition, A.A. All authors have read and agreed to the published version of the manuscript.

Funding: This research was funded by the Los Alamos National Laboratory (LANL).

Institutional Review Board Statement: Not applicable.

Informed Consent Statement: Not applicable.

Data Availability Statement: Data will be made available upon reasonable request.

Acknowledgments: The authors would like to acknowledge the financial support from Los Alamos National Laboratory (LANL). A special thanks to Thomas Burton, Jorge Perez, Sevren Jackson, Devin Binns, Daniel Rhodes, and Kyle Girven for their assistance and fruitful discussions.

Conflicts of Interest: The authors declare no conflicts of interest.

References

1. Braun, S.; Ewins, D.; Rao, S.; Leissa, A. Encyclopedia of vibration: Volumes 1, 2, and 3. *Appl. Mech. Rev.* **2002**, *55*, B45. [CrossRef]
2. Keightley, W.O. Vibration Tests of Structures. Doctoral Dissertation, California Institute of Technology, Pasadena, CA, USA, 1964.
3. Takeshita, A.; Madrid, J.; Granillo, E.; Abdelkefi, A. Insights on the impacts of accelerometer location on the dynamics and characteristics of complex structures. *Sensors* **2023**, *23*, 9830. [CrossRef] [PubMed]
4. Chen, G.; Li, Q.-Y.; Li, D.-Q.; Wu, Z.-Y.; Liu, Y. Main frequency band of blast vibration signal based on wavelet packet transform. *Appl. Math. Model.* **2019**, *74*, 569–585. [CrossRef]
5. Chen, G.; Yang, J.; Liu, Y.; Kitahara, T.; Beer, M. An energy-frequency parameter for earthquake ground motion intensity measure. *Earthq. Eng. Struct. Dyn.* **2022**, *52*, 271–284. [CrossRef]
6. Varoto, P.S. Issues in laboratory simulation of field vibration data: Experimental results on a typical structure. In *Sensors and Instrumentation, Aircraft/Aerospace, Energy Harvesting & Dynamic Environments Testing, Volume 7: Proceedings of the 37th IMAC, A Conference and Exposition on Structural Dynamics, Orlando, FL, USA, 28–31 January 2019*; Springer International Publishing: Berlin/Heidelberg, Germany, 2020; pp. 347–354.
7. He, R. Airborne Path Frequency Based Substructuring Method and Its Applications. Master's Thesis, University of Kentucky, Lexington, KY, USA, 2015.
8. Dilworth, B.J.; Karlicek, A.; Thibault, L. An approach to component testing: An analytical study. In *Sensors and Instrumentation, Aircraft/Aerospace, Energy Harvesting & Dynamic Environments Testing, Volume 7: Proceedings of the 37th IMAC, A Conference and Exposition on Structural Dynamics, Orlando, FL, USA, 28–31 January 2019*; Springer International Publishing: Berlin/Heidelberg, Germany, 2020; pp. 341–345.
9. de Klerk, D.; Rixen, D.J.; de Jong, J. The frequency based substructuring (FBS) method reformulated according to the dual domain decomposition method. In Proceedings of the 24th International Modal Analysis Conference, A Conference on Structural Dynamics, St. Louis, MO, USA, 30 January–2 February 2006; pp. 1–14.
10. Drozg, A.; Čepon, G.; Boltežar, M. Full-degrees-of-freedom frequency based substructuring. *Mech. Syst. Signal Process.* **2018**, *98*, 570–579. [CrossRef]
11. Law, M.; Ihlenfeldt, S. A frequency-based substructuring approach to efficiently model position-dependent dynamics in machine tools. *Proc. Inst. Mech. Eng. Part K J. Multi-Body Dyn.* **2014**, *229*, 304–317. [CrossRef]

12. de Klerk, D.; Rixen, D.J.; Voormeeren, S.N. General framework for dynamic substructuring: History, review and classification of techniques. *AIAA J.* **2008**, *46*, 1169–1181. [CrossRef]
13. Rixen, D.J. A dual Craig–Bampton method for dynamic substructuring. *J. Comput. Appl. Math.* **2004**, *168*, 383–391. [CrossRef]
14. Krattiger, D.; Wu, L.; Zacharczuk, M.; Buck, M.; Kuether, R.J.; Allen, M.S.; Tiso, P.; Brake, M.R. Interface reduction for Hurty/Craig-Bampton substructured models: Review and improvements. *Mech. Syst. Signal Process.* **2019**, *114*, 579–603. [CrossRef]
15. Bari, N.A.; Serrano, M.; Shenouda, S.M.; Taylor, S.; Schultze, J.; Flynn, G. Quantifying Joint Uncertainties for Hybrid System Vibration Testing. In *Dynamic Substructures, Volume 4: Proceedings of the 38th IMAC, A Conference and Exposition on Structural Dynamics, Houston, TX, USA, 10–13 February 2020*; Springer International Publishing: Berlin/Heidelberg, Germany, 2021; pp. 131–138.
16. MacNeal, R.H. A hybrid method of component mode synthesis. *Comput. Struct.* **1971**, *1*, 581–601. [CrossRef]
17. Lion, P.M. Rapid identification of linear and nonlinear systems. *AIAA J.* **1967**, *5*, 1835–1842. [CrossRef]
18. Baur, U.; Benner, P.; Feng, L. Model Order Reduction for Linear and Nonlinear Systems: A System-Theoretic Perspective. *Arch. Comput. Methods Eng.* **2014**, *21*, 331–358. [CrossRef]
19. Elliott, S.J.; Tehrani, M.G.; Langley, R.S. Nonlinear damping and quasi-linear modelling. *Philos. Trans. R. Soc. A Math. Phys. Eng. Sci.* **2015**, *373*, 20140402. [CrossRef] [PubMed]
20. Nayfeh, A.H.; Mook, D.T. *Nonlinear Oscillations*; John Wiley & Sons: Hoboken, NJ, USA, 2008.
21. Touzé, C.; Thomas, O.; Chaigne, A. Hardening/softening behaviour in non-linear oscillations of structural systems using non-linear normal modes. *J. Sound Vib.* **2004**, *273*, 77–101. [CrossRef]
22. Soine, D.E.; Jones, R.J.; Harvie, J.M.; Skousen, T.J.; Schoenherr, T.F. Designing hardware for the boundary condition round robin challenge. In *Topics in Modal Analysis & Testing, Volume 9: Proceedings of the 36th IMAC, A Conference and Exposition on Structural Dynamics, Orlando, FL, USA, 12–15 February 2018*; Springer International Publishing: Berlin/Heidelberg, Germany, 2019; pp. 119–126.
23. Harvie, J.M.; Schoenherr, T.F.; Skousen, T.J. *Boundary Conditions in Environmental Testing Round Robin (No. SAND2018-1275C)*; Sandia National Lab. (SNL-NM): Albuquerque, NM, USA, 2018.
24. Takeshita, A.; Sedillo, H.; Jankowski, K.; Barba, J.; Bouma, A.; Billingsley, E.; Abdelkefi, A. Effects of test fixture connections and interference of the BARC structure on its dynamical responses. *Int. J. Mech. Sci.* **2022**, *221*, 107186. [CrossRef]
25. Bouma, A.; Campbell, A.; Roberts, T.; Taylor, S.; Haynes, C.; Harvey, D. Accumulated lifetimes in single-axis vibration testing. In *Sensors and Instrumentation, Aircraft/Aerospace, Energy Harvesting & Dynamic Environments Testing, Volume 7: Proceedings of the 37th IMAC, A Conference and Exposition on Structural Dynamics, Orlando, FL, USA, 28–31 January 2019*; Springer International Publishing: Berlin/Heidelberg, Germany, 2020; pp. 131–146.
26. Musella, U.; Blanco, M.A.; Mastrodicasa, D.; Monco, G.; Emilio, D.L.; Simone, M.; Mucchi, E.; Guillaume, P. Combining test and simulation to tackle the challenges derived from boundary conditions mismatches in environmental testing. In *Sensors and Instrumentation, Aircraft/Aerospace, Energy Harvesting & Dynamic Environments Testing, Volume 7: Proceedings of the 37th IMAC, A Conference and Exposition on Structural Dynamics, Orlando, FL, USA, 28–31 January 2019*; Springer International Publishing: Berlin/Heidelberg, Germany, 2020; pp. 259–269.
27. Schoenherr, T.F.; Clark, B.W.; Coffin, P. *Improve Replication of in-Service Mechanical Environments (No. SAND2018-10187)*; Sandia National Lab. (SNL-NM): Albuquerque, NM, USA, 2018.
28. Granillo, E.C.; Madrid, J.M.; Padilla, C.L.; Perez, J.; Abdelkefi, A. Insights on the scalability of the BARC structure on its dynamical characteristics. In Proceedings of the AIAA Scitech 2024 Forum, Orlando, FL, USA, 8–12 January 2024.
29. Rohe, D.P.; Schultz, R.A.; Schoenherr, T.F.; Skousen, T.J.; Jones, R.J. Comparison of multi-axis testing of the BARC structure with varying boundary conditions. In *Sensors and Instrumentation, Aircraft/Aerospace, Energy Harvesting & Dynamic Environments Testing, Volume 7: Proceedings of the 37th IMAC, A Conference and Exposition on Structural Dynamics, Orlando, FL, USA, 28–31 January 2019*; Springer International Publishing: Berlin/Heidelberg, Germany, 2020; pp. 179–193.
30. Rohe, D.P. *Modal Data for the BARC Challenge Problem Test Report (No. SAND-2018-0640R)*; Sandia National Lab. (SNL-NM): Albuquerque, NM, USA, 2018.
31. Rohe, D.P.; Smith, S.; Brake, M.R.; DeClerck, J.; Blanco, M.A.; Schoenherr, T.F.; Skousen, T.J. Testing summary for the box assembly with removable component structure. In *Sensors and Instrumentation, Aircraft/Aerospace, Energy Harvesting & Dynamic Environments Testing, Volume 7: Proceedings of the 37th IMAC, A Conference and Exposition on Structural Dynamics, Orlando, FL, USA, 28–31 January 2019*; Springer International Publishing: Berlin/Heidelberg, Germany, 2020; pp. 167–177.
32. Schoenherr, T.F. *Designing an Optimized Fixture for the BARC Hardware Using a Parameterized Model (No. SAND2019-12838C)*; Sandia National Lab. (SNL-NM): Albuquerque, NM, USA, 2019.
33. Padilla, C.L.; Madrid, J.M.; Granillo, E.C.; Flores, A.; Abdelkefi, A. Dynamics and nonlinear characterization of BARC systems with varying central cut widths. In Proceedings of the AIAA SCITECH 2024 Forum, Orlando, FL, USA, 8–12 January 2024.
34. Lu, K.; Jin, Y.; Chen, Y.; Yang, Y.; Hou, L.; Zhang, Z.; Li, Z.; Fu, C. Review for order reduction based on proper orthogonal decomposition and outlooks of applications in mechanical systems. *Mech. Syst. Signal Process.* **2019**, *123*, 264–297. [CrossRef]

35. Paripovic, J.; Mayes, R.L. Reproducing a component field environment on a six degree of-freedom shaker. In *Dynamic Substructures, Volume 4: Proceedings of the 38th IMAC, A Conference and Exposition on Structural Dynamics, Houston, TX, USA, 10–13 February 2020*; Springer International Publishing: Berlin/Heidelberg, Germany, 2021; pp. 73–78.
36. Cooper, S.B.; DiMaio, D.; Ewins, D.J. Integration of system identification and finite element modelling of nonlinear vibrating structures. *Mech. Syst. Signal Process.* **2018**, *102*, 401–430. [CrossRef]
37. Avitabile, P. *Modal Testing: A Practitioner's Guide*, 5th ed.; The Society for Experimental Mechanics; John Wiley & Sons Ltd.: Hoboken, NJ, USA, 2018.

Disclaimer/Publisher's Note: The statements, opinions and data contained in all publications are solely those of the individual author(s) and contributor(s) and not of MDPI and/or the editor(s). MDPI and/or the editor(s) disclaim responsibility for any injury to people or property resulting from any ideas, methods, instructions or products referred to in the content.